https://doi.org/10.5194/egusphere-2026-1893
Preprint. Discussion started: 14 April 2026

Orographic impacts of Réunion Island and Madagascar on heavy rainfall during Tropical Cyclone Batsirai (2022)

Keun-Ok Lee[1], Soline Bielli[2], Clément Soufflet[1], Rémi Laxenaire[1] and Kevin Hoarau[1]
[1]Laboratoire de l'Atmosphère et des Cyclones, UMR 8105, CNRS, Université de La Réunion, Météo-France, Saint-Denis, La Réunion, France
[2]Centre National de Recherches Météorologiques, Université de Toulouse, Météo-France, CNRS, Toulouse, France
Correspondence to: Keun-Ok Lee (keunok.lee@cnrs.fr)

Abstract. During the passage of tropical cyclone (TC) Batsirai (2022), the mountainous regions of Réunion Island and the eastern part of Madagascar experienced devastating floods. TC Batsirai passed north of Réunion Island (minimum distance of ~210 km) before making landfall along the eastern coast of Madagascar. Using the Meso-NH model at 2 km resolution, we conducted a control simulation with realistic topography (CTL) and three flattened-terrain experiments (FLT_{all}, FLT_{mdg}, and FLT_{reu}) to assess orographic effects. Results show that the terrain of Réunion and Madagascar enhanced localized rainfall by 94% (2,800 mm) and 82% (830 mm), respectively. Over Réunion Island, orographically uplifted low-level moisture sustained 60 h of heavy rainfall (10 mm h^{-1}), with a peak of 96 mm h^{-1}, although the cyclone's intensity and track were minimally affected. In Madagascar, terrain not only intensified precipitation (19 h of heavy rainfall with a peak intensity of 92.8 mm h^{-1}) but also altered the TC trajectory, delaying landfall by about 12 h and shifting it approximately 30 km south. These findings highlight the critical role of complex orography in shaping localized rainfall and TC behaviour in the southwest Indian Ocean.

1 Introduction

Tropical cyclones (TCs) are highly destructive meteorological phenomena, particularly for mountainous islands and coastal regions. These regions are especially vulnerable and can experience severe impacts, including strong winds, heavy rainfall-induced flooding, and storm surge (Roux et al., 2004). In many TC-affected areas, interactions between TC circulations and local topography are recognized as key processes that contribute to prolonged and torrential rainfall. The increased water vapor content and enhanced thermodynamic energy associated with TCs have therefore raised substantial concerns regarding hydrometeorological hazards in mountainous regions (Hamuro et al., 1969; Parrish et al., 1982; Wu et al., 2016; Huang et al., 2020; Cheng et al., 2025).

The influence of mountainous islands on TC structure and intensity has been extensively studied in Taiwan, where the southwest-northeast-oriented Central Mountain Range (CMR; about 300 km long, 100 km wide, 3,500 m high) strongly modulates not only total rainfall but also the track and intensity of approaching and/or landfalling TCs (Bender et al., 1985,1987; Yeh and Elsberry, 1993a, 1993b; Wu and Kuo, 1999; Wu, 2001; Lin et al., 2005; Yu and Cheng, 2014; Wu et al., 2016; Lin et al., 2020; Wu et al., 2022). Regarding rainfall, numerous studies have shown that the steep terrain of CMR plays

https://doi.org/10.5194/egusphere-2026-1893
Preprint. Discussion started: 14 April 2026

a pivotal role in enhancing total rainfall accumulation and shaping its spatial distribution through orographically modified low-level winds (Chang et al., 1993; Yu and Cheng, 2014; Huang et al., 2020). For example, during Typhoon Morakot (2009), more than 2,885 mm of rainfall—exceeding the mean annual precipitation—was recorded over 100 hours in southern Taiwan as the typhoon traversed the CMR, producing a striking contrast with rainfall in the northern CMR. By combining observational analyses with numerical simulations, Lin et al. (2011) identified key multiscale mechanisms responsible for the localized extreme rainfall: (i) enhanced large-scale low-level convergence involving the northerly components of the typhoon circulation and the southwesterly monsoonal flow, further intensified by blocking along the steep mountain foothills, and (ii) persistent development of fine-scale convective cells within the typhoon's main rainband due to orographic lifting. In parallel, numerous studies have been examined the CMR's influence on TC track deflection. For instance, Lin et al. (2002) reported that strengthened cyclonic northerly winds west of the Typhoon Megi (2016) centre, ahead of and over the CMR, contributed to a southward deflection of the TC track. Detailed diagnostics of the potential vorticity tendency budget from coupled ocean-atmosphere simulations further revealed that this southward deflection was driven by southeastward tendencies associated with latent heating near landfall. Additionally, they found that TC motion slowed near landfall primarily due to the formation of a low-level cold pool generated by strong rainfall along the mountain slopes.

TCs forming in the southwest Indian Ocean (SWIO) frequently affect mountainous island nations such as Madagascar (approximately 1,600 km long, 600 km wide, and 2,800 m high; Fig. 1) and the Mascarene Islands, including Réunion Island (63 km long, 45 km wide, 3,070 m high) and Mauritius (61 km long, 46 km wide, 600 m high). Similar to situations observed in Taiwan, these islands often experience substantial orographic modulation of TC dynamics, resulting in notable alterations to TC track, intensity, and rainfall. In the Madagascar region—where the terrain is approximately five times larger in horizontal extent than the CMR of Taiwan but exhibits a similar southwest-northeast orientation—a few studies have examined landfalling TCs and their associated impacts, particularly in coastal areas (Needham et al., 2015; Arivelo and Lin, 2016; Rakotoarimanana et al., 2022; Khan et al., 2025). Due to its geographical position, the rainfall features of Madagascar are largely modulated by the Intertropical Convergence Zone (ITCZ), which exhibits synoptic-scale fluctuations associated with complex northeasterly and southeasterly trade-wind systems, accompanied by bands of convective clouds and precipitation (Hastenrath and Lamb, 1978; Grodsky and Carton, 2003). More importantly, variations in rainfall amounts over Madagascar are strongly influenced by TCs, a relationship closely tied to the position and intensity of the ITCZ (Duchiron, 2002). In addition, Fitchett and Grab (2014) noted that Madagascar's mountainous topography acts as a land shield for many intense TCs that develop in this region, contributing to orographic rainfall production. Arivelo and Lin (2016) further investigated orographic rainfall over Madagascar using Froude number (*Fr*) analyses, showing that during the austral summer, *Fr* values typically range from 0.88 to 1.16. Such reduced *Fr* values indicate strong flow blocking, which enhances the likelihood of heavy rainfall, particularly when a moist system such as a TC contains high available potential energy.

Compared with Madagascar, the orography of Réunion Island is small, more circular in shape, and characterized by much steeper terrain (Fig. 1). Several studies have investigated the orographic influence of Réunion Island on TC track and intensity (Roux et al., 2004; Jolivet et al., 2013; Barbary et al., 2018). Jolivet et al. (2013) showed that the presence of the island slowed

https://doi.org/10.5194/egusphere-2026-1893
Preprint. Discussion started: 14 April 2026

the intensification of landfalling TC Dina (2002), which passed close to the coast with a minimum distance of 65 km, ultimately resulting in a weaker system. Their sensitivity experiments—with and without the island's real topography—suggested that the horizontal circulation of the TC was strongly modulated by orographic forcing. They further reported that the circular and mountainous shape of the island acted to stabilize the cyclonic circulation by damping the natural elliptical rotation of the eyewall and constraining the flow during landfall. Using a series of idealized numerical experiments, Barbary et al. (2018) examined the potential influence of a small island such as Réunion on TC behaviour and quantified the distance at which such interaction becomes significant, depending on the approaching TC's direction and translation speed. Their results indicated detectable impacts on TC track up to 150–200 km from the island and on TC intensity up to 50 km. These effects became more pronounced when TC passed within 50 km of the island, occasionally leading to episodic intensification.

These previous studies provide clear evidence that the orography of Madagascar and Réunion Island can modulate the track and intensity of approaching TCs; however, their role in modulating rainfall has not yet been thoroughly investigated. In particular, the influence of large scale terrain such as that of Madagascar on TC track and intensity—and its subsequent impact on local rainfall—remains insufficiently explored. In this study, using both observational data and a high-resolution numerical model, we aim to improve our understanding of the orographic effects of Madagascar and Réunion Island on approaching TC track, intensity, and, ultimately, heavy rainfall. To do so, we focus on a representative case: TC Batsirai (2022).

Batsirai was the most intense system of the 2021–2022 cyclone season in the SWIO. It propagated southwestward, affecting the Mascarene Islands and eastern Madagascar (black line, Fig. 1). Batsirai reached the intensity of an intense tropical cyclone on the SWIO scale—equivalent to Category 4 on the Saffir-Simpson scale (Kantha, 2006)—with a minimum sea-level pressure (MSLP) of 932 hPa at 12 UTC on 2 February, shortly after passing north of Mauritius (indicated by a red arrow, Fig. 1). Réunion Island experienced agricultural losses of approximately USD 47 million, primarily due to flooding (Le Quotidien, 2022). The most devastating impacts occurred in Madagascar, especially along the eastern coastal region. More than 112,000 people were displaced by flooding, 121 fatalities were reported, and widespread power outages, as well as severe economic, agriculture, and infrastructure losses, were documented (OCHA, 2022; Khan et al., 2025).

Section 2 provides a brief introduction to TC Batsirai, along with descriptions of the observational datasets and numerical model. Section 3 validates the simulated lifecycle of TC Batsirai using multiple observational datasets. Section 4 then presents a detailed analysis of the orographic influence on TC track and intensity, followed by an examination of the resulting intense rainfall. Finally, Section 5 offers concluding remarks from the present study.

https://doi.org/10.5194/egusphere-2026-1893
Preprint. Discussion started: 14 April 2026

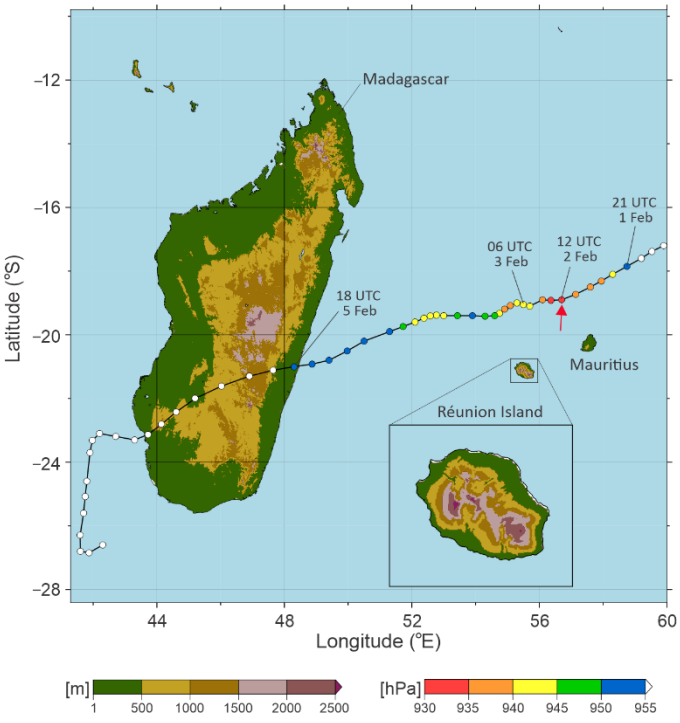

Figure 1. Topography of the SWIO region and the observed trajectory of TC Batsirai (2022) from IBTrACS. Three-hourly minimum sea level pressure (MSLP) values are indicated by colored circles along the black solid line. The location and timing of the cyclone's minimum MSLP (12 UTC on 2 February 2022) are highlighted with a red arrow.

2 Data and method

2.1 Tropical Cyclone Batsirai (2022)

The genesis of Batsirai occurred on 23 January 2022 in the SWIO. It was first classified as a tropical cyclone at 03 UTC on 25 January by the Joint Typhoon Warning Centre (JTWC) and the Regional Specialized Meteorological Centre (RSMC) La Réunion reported 3 hours later that the system had intensified into a moderate tropical storm (17 m $s^{-1} \leq V_{max} <$ 24 m s^{-1}) on the RSMC La Réunion scale. The system moved rapidly westward, undergoing several cycles of intensification and weakening until 1 February. At 18 UTC on 1 February 2022, Batsirai strengthened into a tropical cyclone (33 m $s^{-1} \leq V_{max} <$ 43 m s^{-1}) on the RSMC La Réunion scale (Fig. 1), and by 03 UTC on 2 February it experienced a period of rapid intensification, reaching intense tropical cyclone status ($V_{max} \geq$ 44 m s^{-1}), equivalent to Category 4 Saffir-Simpson scale. At 12 UTC on 2 February, Batsirai reached its minimum sea-level pressure to 932 hPa (indicated by a red arrow, Fig. 1) north of Mauritius. After reaching peak intensity, RSMC La Réunion reported a brief weakening associated with an eyewall replacement cycle (ERC) that occurred north of Mauritius and Réunion Island. Upon completing the ERC, the system underwent a short-lived re-intensification (minimum pressure of 934 hPa).

https://doi.org/10.5194/egusphere-2026-1893
Preprint. Discussion started: 14 April 2026

Beginning on 2 February, Batsirai brought heavy rainfall to Réunion Island as it passed to the north of the island with a minimum sea-level pressure of around 940 hPa. Its closest approach was approximately 210 km at around 06 UTC on 3 February (Fig. 1). Both operational radar and rain-gauge observations indicated accumulated amount exceeding 1800 mm over the mountainous regions where terrain elevation surpass 500 m during the subsequent three days (Fig. 2). The area of intense rainfall (greater than 500 mm over three days) closely follows the contours of the island's topography (Fig. 1), a phenomenon often referred to as "phase locking by terrain", which has also been often observed in CMR of Taiwan during typhoon season (Wu and Kuo, 1999; Huang et al., 2020). Although individual event may exhibit strong geometric asymmetry in rainfall distribution, statistical analyses reveal that such asymmetry can be largely reduced, highlighting the dominant influence of slope steepness regardless of whether the area is upwind or downwind. On Réunion Island, this terrain-locked rainfall pattern has been often documented during the passage of tropical cyclones.

After Batsirai passed Réunion Island, it underwent another series of intensification and weakening cycles while maintaining its overall convective structure, until it made landfall along the eastern coast of Madagascar (Fig. 1). Batsirai made landfall with a minimum sea-level pressure to 952 hPa at approximately 15 UTC on 5 February, followed by rapid decay due to land interaction.

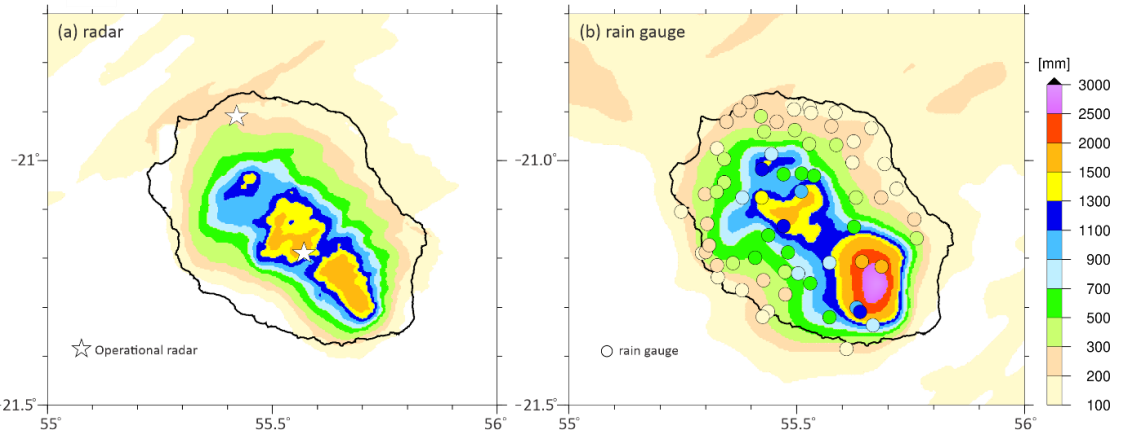

Figure 2. Three-day accumulated precipitation over Réunion Island from 00 UTC on 2 February to 00 UTC on 5 February 2022. Panel (a) shows radar observations with the two operational radars indicated by stars. Panel (b) shows rain gauge observations (colored circles for stations with precipitation ≥ 100 mm) and the CTL simulation (shaded).

2.2 Operational observation

The IBTrACS (International Best Track Archive for Climate Stewardship) version 4r01 (Gahtan et al., 2024) best-track data were used to determine the location and intensity of TC Batsirai (Figs. 1, 3 and 4). IBTrACS is the result of a globally coordinated and collaborative effort that provides a centralized repository of global TC best-track data from the RSMCs and other agencies. IBTrACS data contains numerous inhomogeneities in intensity records due to interagency differences in

https://doi.org/10.5194/egusphere-2026-1893
Preprint. Discussion started: 14 April 2026

available technologies, observations, and procedures over time. For example, the qualitative uncertainty for intensity in wind speed for TCs in the South Indian Ocean basin is estimated at approximately ±10 knots for systems that developed after 1995 (Knapp et al., 2010; Gahtan et al., 2024). Regarding position, storm locations are generally reported with a resolution of 0.1°, resulting in a lower bound of positional uncertainty of approximately 10 km. Kruk et al. (2010) also found that the spatial uncertainty varies with storm intensity, likely because weaker storms have broader and less well-defined centres of circulation than systems with clear eyes. Gahtan et al. (2024) estimated a positional uncertainty of approximately 10−15 km for strong TCs (wind ≥ 100 knots) such as Batsirai. The IBTrACS data used in this study are provided at 3-hourly intervals, except for data missing at 21 UTC on 2 February and 03 UTC on 5 February.

To evaluate the spatial and temporal distribution of rainfall over Réunion Island, we employed operational datasets from Météo-France, including hourly rainfall observations from 75 ground-based rain gauges and near-surface composite rainfall at 5-min intervals (250 m horizontal resolution) from two C-band Doppler radars. The locations of the rain gauges and radars are indicated by circles and star marks, respectively in Figure 2. Three-days accumulated from rain gauges and radar composite data was used to evaluate the rainfall produced by the numerical simulations.

Near-surface wind data were obtained from high-resolution C-band Synthetic Aperture Radar (SAR) measurement. SAR, a spaceborne instrument, provides very high-resolution (~1 km) estimates of ocean surface conditions even under extreme weather (Mouche et al., 2019). For extreme weather events, such as TCs, the strong sensitivity of cross-polarized signals to ocean wave breaking has enabled the mapping of ocean surface wind variations at high resolution, including within and around the TC eyes (Mouche et al., 2019; Combot et al., 2020). Previous validation against Stepped Frequency Microwave Radiometer data indicates that SAR-derived wind speeds have a bias of ~1.5 m s^{-1} and a root-mean-square of ~5 m s^{-1} (Mouche et al., 2019). In this study, we used the C-Band SAR Tropical Cyclone Vortex Analysis product at 01:45 UTC on 4 February, which provides a gridded wind field at high resolution, to identify the TC centre and wind distribution and to compare them with numerical simulations.

2.3 Model settings

The non-hydrostatic research model Meso-NH (Lac et al., 2018), version 5.5.0 (http:mesonh.aero.obs-mip.fr/mesonh55) is used in this study to simulate TC Batsirai (2022). The simulation employed approximately 75 million grid points with a horizontal grid spacing of 2 km to resolve fine-scale processes. The vertical grid consisted of 70 stretched levels (Gal-Chen and Somerville, 1975) up to 23 km altitude, with a spacing of 250 m in the free troposphere and 40 m near the surface. The model domain covered the SWIO (2880 km × 1440 km; Fig. 3), encompassing the south-westward passage of Batsirai during the period of 1–5 February 2022. The model time step was set to 5 s. The simulation was initialized at 00 UTC on 1 February, with initial and lateral boundary conditions provided at 6-hour intervals by operational analyses from the European Centre for Medium-Range Weather Forecasts.

The model uses a one-moment bulk microphysics scheme (Pinty and Jabouille, 1998) that predicts six hydrometeor categories: water vapor, cloud water, rainwater, pristine ice, snow, and graupel. Turbulence is parameterized with a 1.5-order

https://doi.org/10.5194/egusphere-2026-1893
Preprint. Discussion started: 14 April 2026

closure of the turbulent kinetic energy equations (Cuxart et al., 2000). In conjunction with the leapfrog temporal scheme, momentum variables are advected using a centred fourth-order scheme, whereas scalar and other meteorological variables were advected with a monotonic Piecewise Parabolic Method to ensure positive definiteness (Colella and Woodward, 1984). At the lateral boundaries, an open-wave radiation condition combined with a five-grid-point relaxation flow scheme (Davies, 1976) is applied. Radiation processes are presented by the Rapid Radiation Transfer Model (Mlawer et al., 1997), and surface fluxes are computed using the SURFEX platform (Masson et al., 2013).

2.4 Numerical experiments

In this study, to investigate the orographic effect on localized heavy precipitation during the passage of TC Batsirai (2022), we conducted one set of sensitivity experiments in addition to a control simulation (CTL) where the terrain was uniformly flattened over (i) the entire model domain (FLT_{all}), (ii) Madagascar only (FLT_{mdg}), and (iii) Réunion Island only (FLT_{reu}) (Table 1). For the CTL run, Meso-NH was configured with realistic topography derived from the Global 30 Arc-Second Elevation dataset (GTOPO30) developed by U.S. Geological Survey. GTOPO30 is a global digital elevation model with a horizontal resolution of 30 arc-seconds (approximately 1 km) and an absolute vertical accuracy of approximately ±30 m. In the sensitivity experiments, the terrain elevations within the designated regions were uniformly reduced to 10 m while all other numerical configurations were identical to those in CTL.

Table 1. List of numerical experiments.

Exp.	horizontal grid spacing	time step	topography	
CTL	2 km	5 s	gtopo30	entire domain
FLT_{all}	〃	〃		entire domain
FLT_{mdg}	〃	〃	flat (z = 10 m)	Madagascar region
FLT_{reu}	〃	〃		Réunion Island

In this study, rainfall rates exceeding 10 mm h^{-1} are used to define the heavy precipitation, while reflectivity values above 45 dBZ are used to identify convective regions. These thresholds are widely used in previous studies on heavy rainfall events (Dyson, 2009; Romatschke, et al., 2010; Lee et al., 2012; 2017). To diagnose the low-level advection of warm, moist air accompanying the tropical cyclone, three-dimensional distribution of equivalent potential temperature (θ_e) from Meso-NH simulation was analyzed (Duffourg et al., 2018; Lee et al., 2018).

3 Evaluation of CTL experiment

3.1 Lifecycle of Batsirai (2022)

The observed and simulated trajectories of TC Batsirai (2022) are shown in Figure 3, and it is evident that the CTL run with a

https://doi.org/10.5194/egusphere-2026-1893
Preprint. Discussion started: 14 April 2026

2 km horizontal grid spacing succeeds in reproducing the TC track. Both IBTrACS-detected (OBS) and CTL-produced Batsirai are located in the SWIO near 62.5°E, 16.5°S at 00 UTC on 1 February (marked by a white dot, Fig. 3), and the system propagated gradually southwestward. Between 00 UTC on 2 February and 00 UTC on 4 February, as TC Batsirai passed adjacent to Mauritius and Réunion Islands (highlighted by a red line, Fig. 3), the CTL track exhibited a slight southward deflection relative to OBS. When TC Batsirai reached the northern offshore region of Réunion Island (marked by yellow dots), the distance between the IBTrACS TC centre and the island's northern coast was ~210 km, while the maximum track discrepancy between OBS and CTL was approximately 70 km around 06 UTC on 3 February. After passing the lee side of Réunion Island, the CTL track shifted westward, rejoining the IBTrACS trajectory around 00 UTC on 4 February. Thereafter, both observed and simulated tracks propagated almost identically toward the eastern coast of Madagascar. In terms of timing, the CTL run made landfall about 3 hours earlier than observation (*i.e.,* 12 UTC *vs*. 15 UTC on 5 February; marked by a light-blue dot). After the landfall (west of ~48.5°E), the CTL-produced Batsirai crossed the steep terrain of Madagascar westward, whereas the IBTrACS track moved west-southwestward.

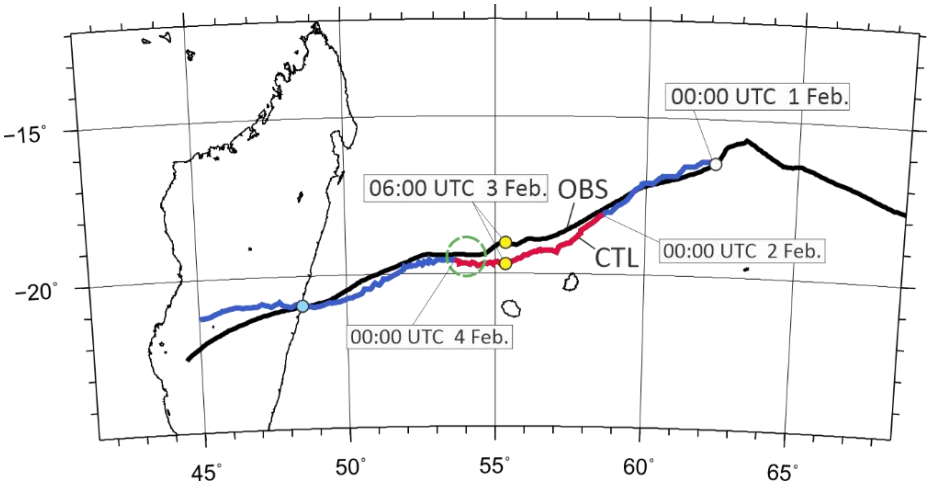

Figure 3. Model domain and observed and simulated tracks of TC Batsirai (2022). The observed IBTrACS track is shown by the black line, while the CTL-simulated track is shown in blue. The highlighted segment (00 UTC 2 February to 00 UTC 4 February) indicates the period of noticeable track discrepancy between CTL and IBTrACS. The white dot marks the initial CTL simulation time (00 UTC 1 February), yellow dots indicate the closest approach of Batsirai to Réunion Island, and the blue dot shows the landfall on the eastern coast of Madagascar.

The intensity changes of TC Batsirai are generally well reproduced by the CTL simulation compared to IBTrACS (Figure 4). Except for the first 6 hours of model spin-up, from 00 UTC on 1 February, both OBS (black line with white dots) and CTL (dark blue line) show a continuous decrease in minimum sea-level pressure (MSLP), reaching their minimum values simultaneously at 12 UTC on 2 February (*e.g.*, 932 hPa for OBS *vs.* 938 hPa for CTL; indicated by a red arrow). However, the

https://doi.org/10.5194/egusphere-2026-1893
Preprint. Discussion started: 14 April 2026

observed rapid intensification over 24 hours from 12 UTC on 1 February (yellow-shaded area), corresponding to an MSLP drop of 32 hPa, is underestimated by the CTL simulation (24.6 hPa). After reaching the minimum MSLP at 12 UTC on 2 February, the MSLP values in both OBS and CTL gradually increased to ~950 hPa by 00 UTC and 06 UTC on 4 February, respectively. Following a short re-intensification (MSLP decreasing to ~940 hPa), the minimum MSLP values of both observed and simulated Batsirai increased again gradually (blue-shaded area) prior to landfall along the eastern coast of Madagascar at approximately 15 UTC (OBS) and 12 UTC (CTL) on 5 February. As soon as TC Batsirai made landfall, the MSLP increased rapidly above 980 hPa. Due to rapid weakening associated with land interaction over Madagascar, the French meteorological administration (*i.e.*, Météo-France) declared that Batsirai had degenerated into an overland depression at 18 UTC on 5 February, while the Joint Typhoon Warning Center downgraded it to a tropical storm. After landfall, Batsirai moved further westward across the terrain in CTL, instead of the southwestward deflection seen in IBTrACS (Fig. 3).

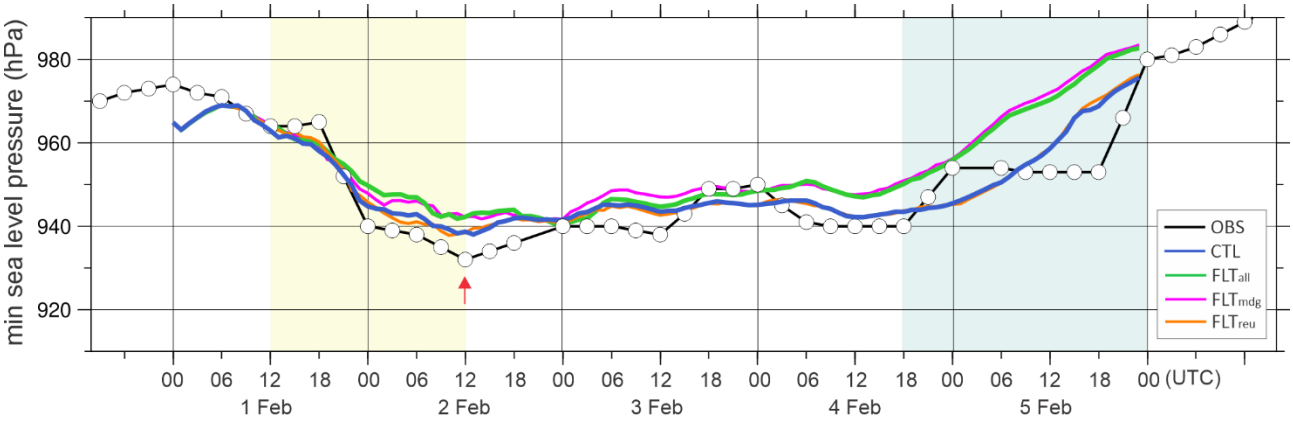

Figure 4. Observed and simulated temporal evolution of minimum sea level pressure (MSLP) for TC Batsirai. Observed 3-hourly MSLP values from IBTrACS are shown as a black line with white circles; note that data at 21 UTC of 2 February and 03 UTC on 5 February are missing. Simulated MSLP values from CTL, FLT_{all}, FLT_{mdg}, and FLT_{reu} are shown in blue, green, magenta, and orange, respectively. The time of minimum observed MSLP is marked by a red upward arrow. Periods of intensification and decay of TC Batsirai are highlighted by yellow and blue shading, respectively.

At 01:45 UTC on 4 February, when TC Batsirai was located near 54.0°E, 19.5°S (marked by a green dashed circle in Fig. 3), with a minimum MSLP of approximately 950 hPa, SAR observations captured near sea-surface winds across the TC system. The SAR-derived 20 m wind profile (black line, Fig. 5) reveals two notable features: (i) a sharp increase in wind speed (from ~12 to 43 m s^{-1}) from the TC centre to the eyewall at a distance of 32 km, and (ii) a gradual decrease in wind speed, nearly having to ~21.3 m s^{-1} at a distance of 200 km from the TC centre. These features are well represented by the CTL simulation (blue line), although CTL produces slightly weaker wind speeds (≤ 5 m s^{-1}) near the TC centre compared to the SAR observations (~12 m s^{-1}). Furthermore, the maximum wind speed (~42 m s^{-1}) in CTL is consistent with the SAR data and is located at the eyewall, with only a small discrepancy in radial distance (~ 20 km; 51 km instead of 32 km). The CTL track

https://doi.org/10.5194/egusphere-2026-1893
Preprint. Discussion started: 14 April 2026

error of approximately 68 km is not critical for this analysis, as Batsirai was sufficiently distant; this displacement corresponds to only a few meters per second in wind speed.

By comparing IBTrACS with CTL in terms of the track and intensity of TC Batsirai, and SAR with CTL in terms of wind speed across the TC system, it is evident that the CTL simulation successfully represents the overall TC lifecycle, including the location and timing of intensity changes as well as the global wind structure.

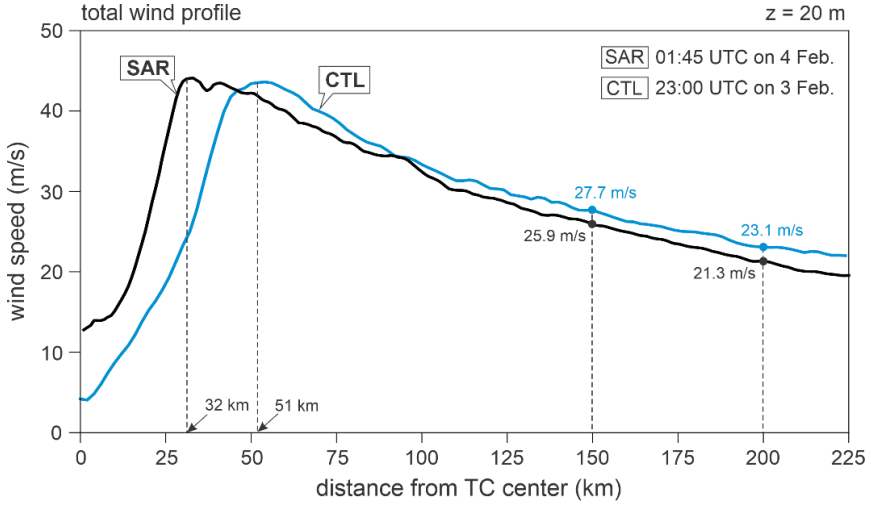

Figure 5. Near-surface wind profiles at 20 m height for TC Batsirai. Observations from SAR at 01:45 UTC on 4 February 2022 are shown as a black solid line, while the CTL simulation at 23 UTC on 3 February 2022 is shown in blue.

3.2 Localized heavy precipitation

While TC Batsirai propagated across the SWIO, Réunion Island experienced prolonged heavy precipitation lasting three days. During this period (2–4 February), Batsirai moved from the northeastern to the northwestern offshore region of the island, with a closest approach of approximately 210 km from the coast. Throughout the TC's propagation, the island was strongly affected by the passage of spiral rainbands associated with the southern sector of the storm. Ground-based operational radar and rain gauge data are used to examine the rainfall characteristics over Réunion Island and to evaluate those produced by the CTL simulation.

The observed and CTL-produced three-day accumulated rainfall distributions are shown in Fig. 2. It is apparent that CTL successfully reproduces the spatial rainfall distribution across the island, namely: (i) a sharp increase in rainfall from the eastern coast toward the central mountainous region, and (ii) localized heavy precipitation over the mountainous area (see Fig. 1 for the orography). A pronounced increase in precipitation, from approximately 100 mm along the eastern coast to more than 1,800 mm in the central to southern mountainous region (maximum of 1,884 mm), is detected in the composite rainfall distribution observed by radar (Fig. 2a), as well as by the rain gauge network (coloured dots in Fig. 2b), which records a maximum value of 1,861 mm. The pronounced contrast in three-day accumulated rainfall between the coastal and mountainous regions, as well

https://doi.org/10.5194/egusphere-2026-1893
Preprint. Discussion started: 14 April 2026

as the substantial precipitation of about 1,500 mm over the central mountainous region, are generally well reproduced by CTL (shaded area in Fig. 2b); however, CTL overestimates the maximum rainfall, with values reaching approximately 2,900 mm in the southern mountainous region. It should also be noted that the rain gauge network in the mountainous region has a relatively coarse spatial resolution.

Although CTL overestimates the maximum rainfall amount in the southern mountainous region, it successfully reproduces the spatial rainfall distribution, particularly the localized heavy precipitation over the mountainous areas, consistent with observations. Further detailed rainfall characteristics associated with the orography of Réunion Island and Madagascar are therefore investigated based on the CTL simulation.

4 Orography effect

By comparing the CTL simulation with the sensitivity experiments—namely FLT_{all}, FLT_{mdg}, and FLT_{reu} (Table 1)—the orographic effects of Réunion Island and eastern Madagascar on the TC track and intensity, as well as the resulting localized heavy precipitation during the passage of TC Batsirai, are comprehensively investigated. The key results are presented in this section.

4.1 Réunion Island

4.1.1 TC trajectory and intensity

An enlarged map showing the observed and simulated trajectories of TC Batsirai from CTL and the sensitivity experiments around Réunion Island (Figure 6a) highlights the orographically modified TC track. All simulations (blue, green, magenta, and orange lines) produce nearly identical trajectories until the system passes north of Mauritius (~57°E) around 09 UTC on 2 February. However, a relatively weaker TC is simulated in FLT_{all} and FLT_{mdg} (minimum MSLP ~942 hPa; green and magenta lines in Fig. 4) compared to CTL and FLT_{reu} (minimum MSLP ~938 hPa; blue and orange lines in Fig. 4). After approximately 12 UTC of 2 February (Fig. 6a), as TC Batsirai propagates north of the region between Mauritius and Réunion Island (section i), the TC in both FLT_{all} and FLT_{mdg} continues to move southwestward, approaching closer to Réunion Island (green arrow). In contrast, the tracks in the other two simulations—CTL and FLT_{reu}—are deflected more westward (blue arrow).

https://doi.org/10.5194/egusphere-2026-1893
Preprint. Discussion started: 14 April 2026

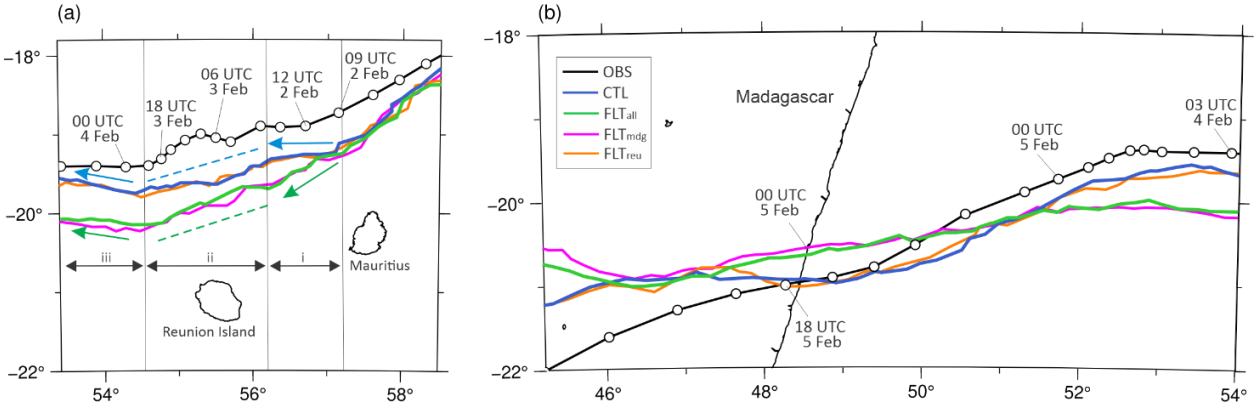

Figure 6. Observed and simulated trajectories of TC Batsirai. The observed track from IBTrACS is shown as a black solid line. Simulated tracks from the CTL, *FLT*$_{all}$, *FLT*$_{mdg}$, and *FLT*$_{reu}$ experiments are shown in blue, green, magenta, and orange solid lines, respectively.

On 3 February, when TC Batsirai moves north of Réunion Island (section ii), all simulations show a general southwestward propagation (blue and green dashed lines in Fig. 6a), with minimum MSLP values ranging from 940 to 950 hPa (Fig. 4). Nevertheless, *FLT*$_{all}$ and *FLT*$_{mdg}$ simulate a weaker TC (minimum MSLP ~950 hPa; green and magenta lines in Fig. 4) compared to CTL and *FLT*$_{reu}$ (minimum MSLP ~945 hPa). Although the overall southwestward motion in section ii is similar across simulations, the distinct track orientations established in section i (westward versus southwestward) lead to differences in proximity to Réunion Island. Consequently, the minimum distance between the TC centre and the northern coast of Réunion Island decreases to ~107 km in *FLT*$_{all}$ and *FLT*$_{mdg}$ around 06 UTC on 3 February, compared to ~145 km in CTL and *FLT*$_{reu}$. On 4 February (section iii), the TC tracks in all simulations shift from southwestward to slightly west-northwestward, in closer agreement with IBTrACS.

Interestingly, the TC evolution simulated in CTL and *FLT*$_{reu}$—in terms of both trajectory and intensity—is nearly identical, suggesting that the terrain effect of Réunion Island on TC Batsirai during its nearby passage is negligible. At the same time, the mesoscale terrain of Madagascar appears to play a crucial role in modifying the track of TC Batsirai, bringing it closer to Réunion Island, whereas its influence on TC intensity in the vicinity is relatively minor.

4.1.2 Precipitation

The five-day accumulated precipitation distributions are shown in Fig. 7. TC-induced precipitation (Fig. 7a) is evident along the storm trajectory, with intense rainfall (~500 mm over five days; blueish areas) in the southern part of the cyclone over the ocean. Two other regions of heavy precipitation are notable: (i) ≥ 800 mm in the mountainous regions of Réunion Island, and (ii) ≥ 500 mm in the southeastern foothills of Madagascar. Over Réunion Island, consistent with Fig. 2b, intense precipitation exceeding ~1,000 mm over three days is confirmed to areas with terrain elevations above 1,000 m, peaking at 3,032 mm on the southern mountain peak. The difference in five-day accumulated precipitation between CTL and *FLT*$_{all}$ (Fig. 7b) indicates

https://doi.org/10.5194/egusphere-2026-1893
Preprint. Discussion started: 14 April 2026

that approximately 94% of the localized heavy precipitation—maximum 2,865 mm—can be attributed to the steep terrain of Réunion Island. Notably, this orographically induced precipitation is confined to mountainous region above 1,000 m (see Fig. 1 for topography). The simulated localized heavy precipitation over the mountainous region of Réunion Island is absent in FLT_{reu}, in a manner nearly identical to FLT_{all}, with the peak precipitation reduced by ~2,900 mm relative to CTL (not shown). Although the simulated TC Batsirai in FLT_{reu} tracks farther north of Réunion Island, nearly identical to CTL (orange line in Fig. 6a), the localized heavy precipitation of approximately 3,000 mm is absent in FLT_{reu}, similar to FLT_{all}. Furthermore, the differences in precipitation over Réunion Island between FLT_{all} and FLT_{mdg}, are negligible, indicating that the terrain effect of Réunion Island is highly localized and does not significantly influence precipitation beyond the island.

A box centered on Réunion Island (55–56°E, 20.8–21.5°S; rectangle in Fig. 7) is used to analyze hourly precipitation over land during the passage of TC Batsirai. The five-day evolution of the maximum hourly precipitation over Réunion Island (Fig. 8a) reveals (i) persistent heavy precipitation (≥ 10 mm h^{-1}) lasting approximately 60 hours in CTL (light blue bars within the grey-shaded period from 18 UTC on 1 February to 07 UTC on 4 February), whereas (ii) only four hours of heavy precipitation are simulated in FLT_{all} (yellow bars from 04 UTC to 07 UTC on 3 February). During this period, the peak hourly precipitation reaches 96 mm h^{-1} in CTL, compared to only 25 mm h^{-1} in FLT_{all}. A sharp increase in hourly precipitation to above 50 mm h^{-1} occurs at 00 UTC on 3 February in CTL, and very intense precipitation (≥ 50 mm h^{-1}) persists for nearly one day while TC Batsirai passes near Réunion Island (section ii marked in Fig. 6a). After 4 February, when the TC moves away from the island, FLT_{all} produces little to no precipitation, whereas CTL continues to simulate weak to intense precipitation ranging from 2 to 30 mm h^{-1}.

https://doi.org/10.5194/egusphere-2026-1893
Preprint. Discussion started: 14 April 2026

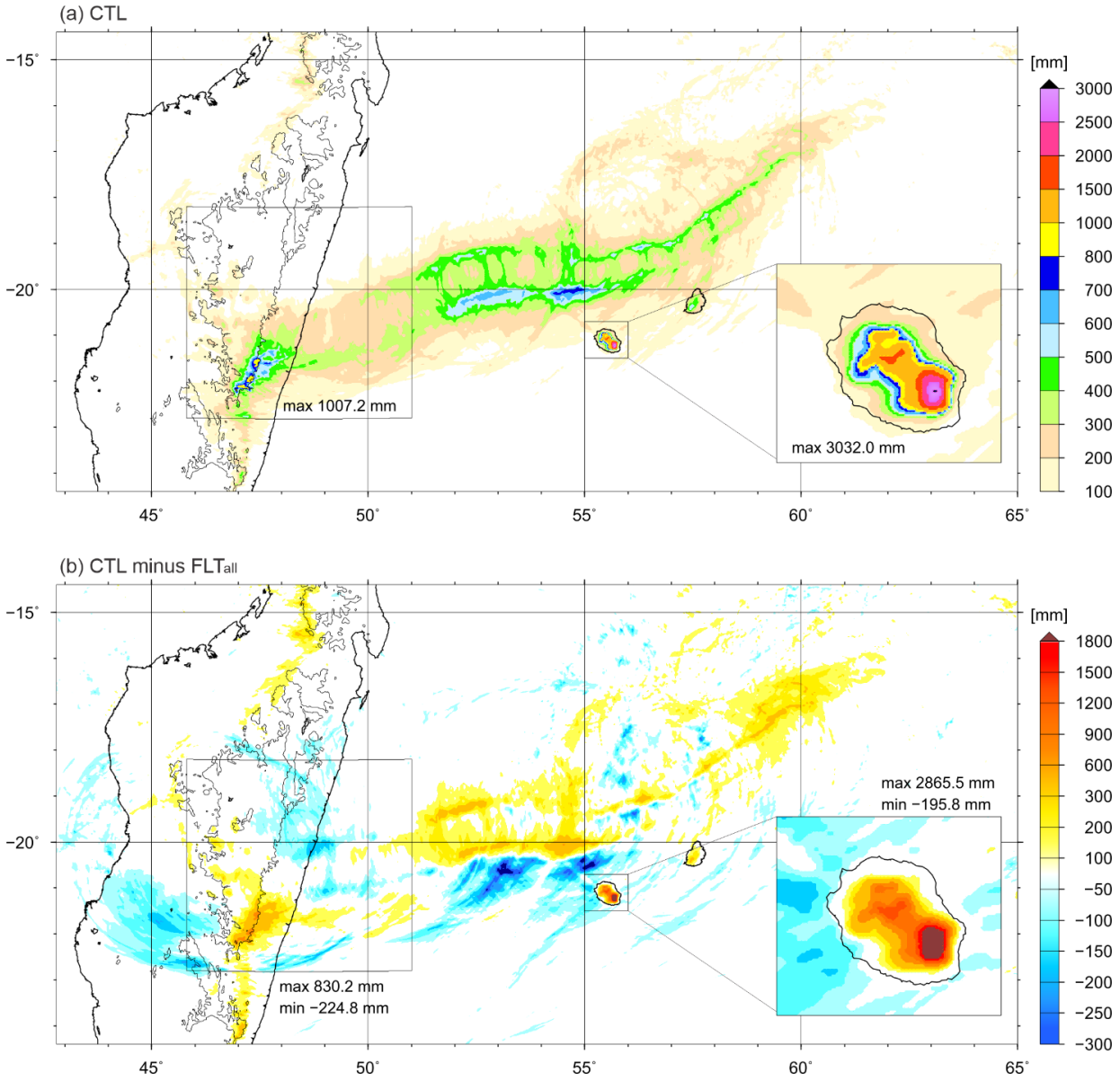

Figure 7. (a) Five-day accumulated precipitation simulated by CTL, and (b) the difference in five-day accumulated precipitation between CTL and *FLT*$_{all}$ experiments (CTL minus *FLT*$_{all}$), starting from 00 UTC on 1 February 2022. The two boxes indicate the analysis domains for the Réunion Island region (55–56°E, 20.8–21.5°S) and the eastern Madagascar region (45.8–51.0°E, 18.2–22.8°S), which are used in Figure 8.

https://doi.org/10.5194/egusphere-2026-1893
Preprint. Discussion started: 14 April 2026

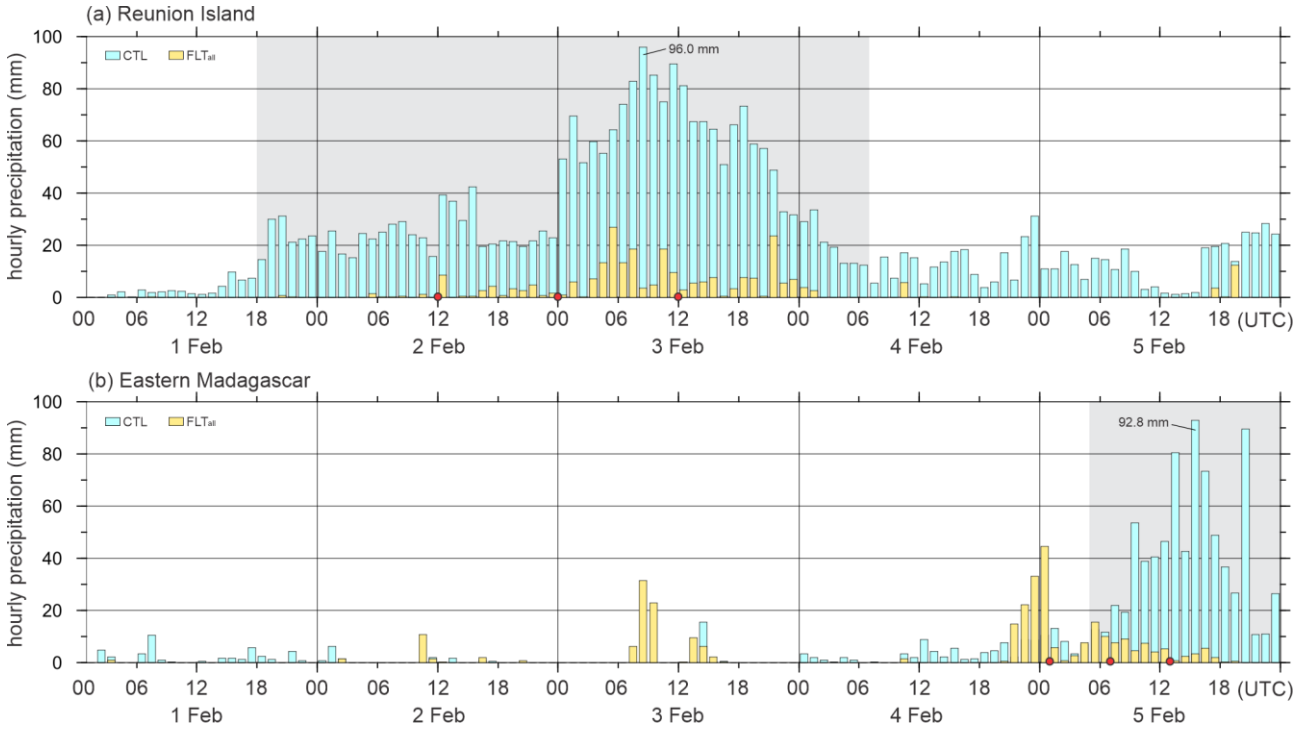

345 **Figure 8. Temporal evolution of the simulated maximum precipitation within the analysis domains over the Réunion Island region (a) and eastern Madagascar region (b) from the CTL (light blue bars) and FLT_{all} (yellow bars) experiments. The horizontal extent of the analysis domains is shown by the boxes in Fig. 7. Red circles along the x-axis indicate the selected times presented in Figs. 9, 10, and 12. The grey-shaded areas highlight period during which precipitation ≥ 10 mm h^{-1} persists.**

350 **4.1.3 Local dynamics**

A comparison between CTL and FLT_{all} (Figs. 4, 6, and 7) clearly demonstrates that the steep orography of Réunion Island critically influences the precipitation distribution, including both five-day accumulated and hourly rainfall. To further investigate the orographically induced low-level winds and moisture fields responsible for the persistent heavy precipitation over Réunion Island, a detailed analysis was conducted. Figure 9 shows the horizontal distributions of reflectivity and low-
355 level moisture flux convergence at three selected times (indicated by red dots on the x-axis of Fig. 8a): 12 UTC on 2 February, prior to the onset of very intense precipitation (exceeding 50 mm h^{-1}) over Réunion Island; 00 UTC on 3 February, corresponding to the onset of very intense precipitation; and 12 UTC of 3 February, during the very intense precipitation period. During this period, the TC eye was located between 18.5°S and 20°S (Figs. 9a–c), while the southern spiral rainbands passed across the island.

360

https://doi.org/10.5194/egusphere-2026-1893
Preprint. Discussion started: 14 April 2026

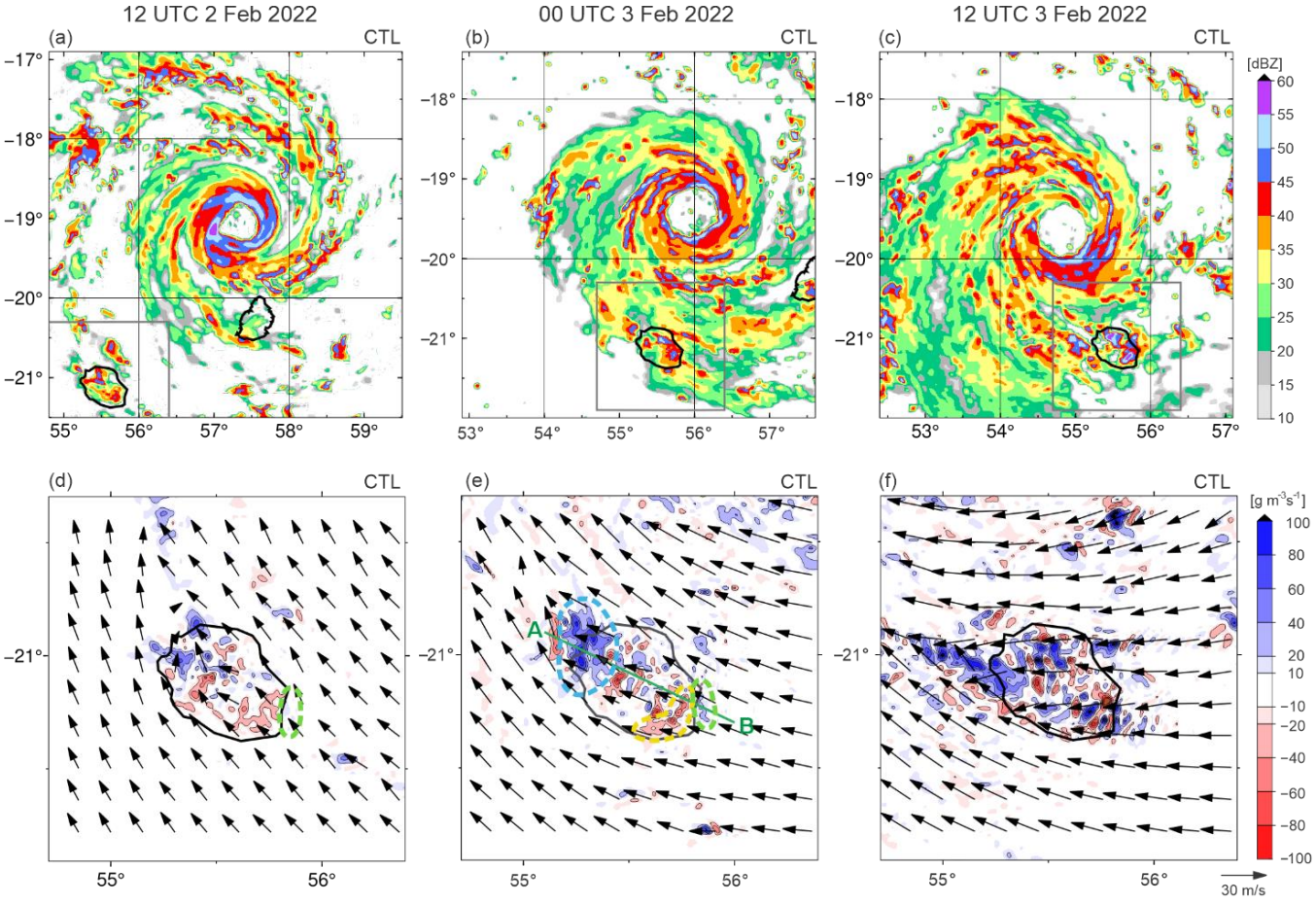

Figure 9. Horizontal distributions of CTL-simulated reflectivity at 3 km above sea level in panels (a)–(c) and low-level moisture flux convergence below 3 km in panels (d)–(f) at 12 UTC on 2 February, 00 and 12 UTC on 3 February 2022. The inner boxes in panels (a)–(c) indicate the domains shown in panels (d)–(f). The green solid line in panel (d) marks the location of the vertical cross-section along A–B used in Fig. 11.

https://doi.org/10.5194/egusphere-2026-1893
Preprint. Discussion started: 14 April 2026

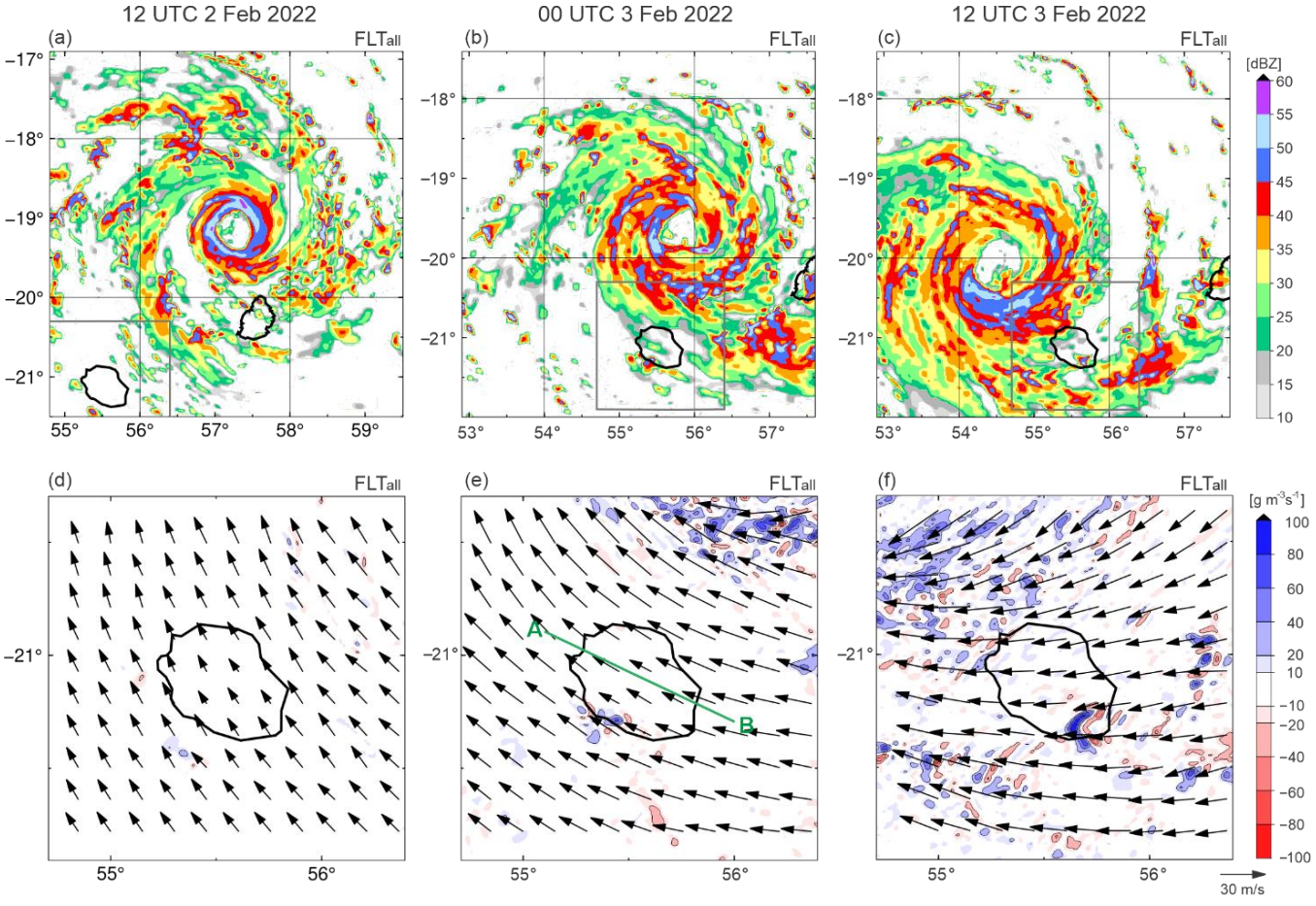

Figure 10. Same as Fig. 9, but showing horizontal distributions of reflectivity at 3 km above sea level (a–c) and low-level moisture flux convergence below 3 km (d–f) from the *FLT$_{all}$* simulation.

At 12 UTC on 2 February, the TC eye was located north of Mauritius, while reflectivity exceeding 25 dBZ was observed over Réunion Island, associated with a thin outer spiral rainband (Fig. 9a). Relatively weak southeasterly flow (8–10 m s^{-1}) prevailed at low altitudes around the island, generating a relatively small Froude number ($Fr \leq 0.3$). Under such small-Fr condition, low-level winds flowed around the terrain, generating two distinct wind structures: (i) divergence (≤ -20 g m^{-3} s^{-1}, red shading in Fig. 9d) on the windward side (*e.g.*, the southeastern foothills) and (ii) convergence (≥ 40 g m^{-3} s^{-1}, blue shading) on the lee side (*e.g.* the northwestern slope). Another notable feature is that the ambient low-level southeasterlies converge with the deflected flow along the eastern coast (delineated by the green dashed line). In contract, these wind structures are absent in *FLT$_{all}$* at the same time (Figs. 10a, d). Although the TC is located north of Mauritius, similar to CTL, and relatively weak southeasterlies prevail at low levels, Réunion Island remains relatively calm in *FLT$_{all}$*.

At 00 UTC on 3 February, the TC approached closer to Réunion Island, and more pronounced convective regions with

https://doi.org/10.5194/egusphere-2026-1893
Preprint. Discussion started: 14 April 2026

reflectivity exceeding 45 dBZ are evident over the southeastern and northern mountainous regions of the island at an altitude of 3 km (Fig. 9b), accompanied by a complex pattern of moisture convergence and divergence at low levels (Fig. 9e), similar to that seen at previous time (Fig. 9d) but with increase intensity. With TC approach, further intensified low-level southeasterlies (10–20 m s^{-1}) prevailed around the island, with *Fr* increasing to ~0.4. The flow partially split and moved around the mountain foothills, resulting in (i) a rounded region of moisture divergence (≤ –50 g m^{-3} s^{-1}, delineated by the yellow dashed contour) on the windward side near the foothills, and (ii) a strong moisture convergence region (≥ 80 g m^{-3} s^{-1}, delineated by the blue dashed contour) on the lee side. On the windward side, the partially split low-level flow continuously converges with the environmental southeasterlies, leading to localized moderate moisture convergence (~20 g m^{-3} s^{-1}, blue shading) along the southeastern coast, as outlined by the green dashed contour in Fig. 9e. These dynamical features correspond well with the enhanced reflectivity observed over the mountainous terrain.

In contrast, the strong reflectivity cores and organized low-level moisture flux patterns evident in CTL at 00 UTC are absent in FLT_{all} at the same time (Figs.10b, e). Although the simulated TC in FLT_{all} approaches approximately 35 km closer to the island, with the TC center located between 19.5° and 20.5°S (Figs. 10a–c), the reflectivity over the island remains weak and fragmented (< 35 dBZ). Meanwhile, nearly identical dynamical features are identified in FLT_{reu} as in FLT_{all}, despite the difference in TC proximity (not shown).

The vertical cross-sections along the A-B line of equivalent potential temperature (θ_e) and vertical wind (Fig. 11) indicate that low-level warm and moist air ($\theta_e \geq 350$ K) is partially uplifted along the windward mountain slope from below 500 m to above 2.5 km. Very high θ_e values (≥ 356 K) extend from the southeastern coast to the mountain summit (~1.8 km). The uplifted warm and moist air ($\theta_e \geq 350$ K) reaches altitudes up to 4 km above the mountain crest, while a deeper moist layer, extending to about 5 km, is evident on the lee side (*i.e.*, northwestern offshore of the island), where pronounced orographically induced moisture flux convergence occurs (delineated by the blue dashed contour in Fig. 9e). In addition to the partially deflected flow around the terrain and the associated wind convergence on the lee side, descending motion is also apparent along the downwind slope. The combined effects of low-level wind convergence and vertical uplift, likely enhanced by accelerated gravity-wave dynamics on the lee side, appear to play a crucial role in deepening the moist layer downstream of the island.

https://doi.org/10.5194/egusphere-2026-1893
Preprint. Discussion started: 14 April 2026

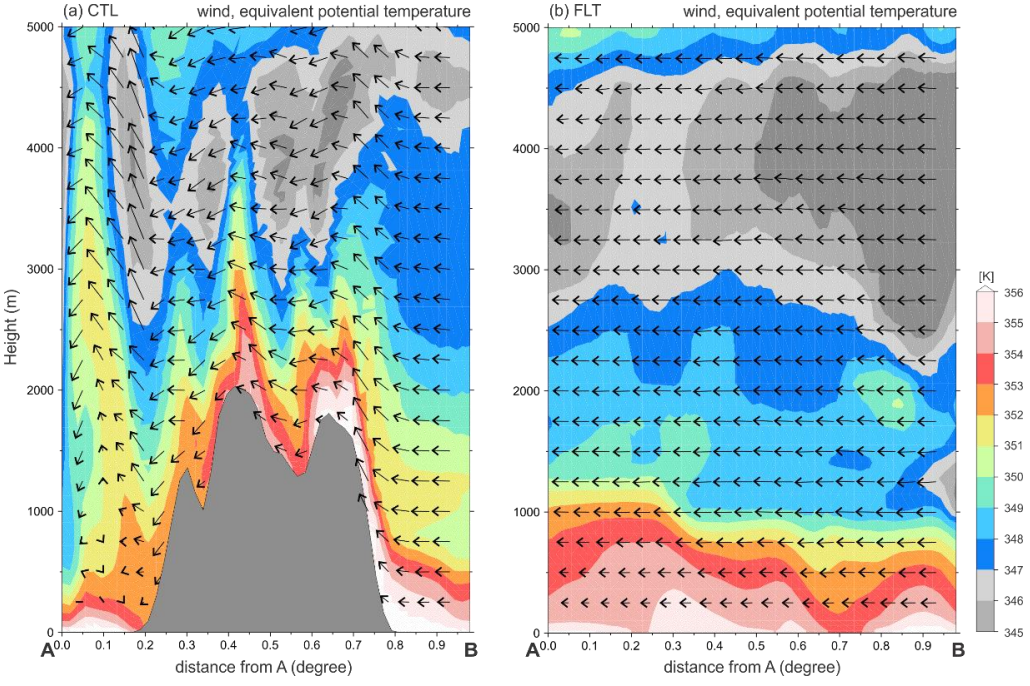

Figure 11. Vertical cross-sections of wind (u–w vectors) and equivalent potential temperature (θ_e, shaded) along the A–B line, simulated by (a) CTL and (b) FLT_{all} at 00 UTC on 3 February. The location of the A–B line is shown by the green solid line in Figs. 9d and 10d for the CTL and FLT_{all} simulations, respectively. The grey-shaded area in (a) represents the topography.

In contrast, in FLT_{all} (Fig. 11b), the warm and moist air ($\theta_e \geq 352$ K) remains confined below 1 km, and is distributed relatively homogeneously along the cross-section, with a drier air mass ($\theta_e \leq 350$ K) above. The vertical structures of θ_e and vertical wind resemble those simulated in FLT_{reu} (not shown). The comparison between CTL and FLT_{all} (Fig. 11) clearly demonstrates that the high terrain of Réunion Island plays a critical role in lifting the abundant low-level moisture advected by TC Batsirai to altitudes above 4 km on the windward side and near the mountain crest, thereby contributing to the intense precipitation over the mountainous region.

During 00–12 UTC on 3 February, spiral rainbands continued to pass over the island in CTL (Figs. 9b–c), and convective regions (reflectivity ≥ 45 dBZ) persisted over the mountainous areas. Compared with the reflectivity distribution at 12 UTC on 2 February (Fig. 9a), the spiral rainbands became further thickened, and the convective regions within the rainbands expanded by 12 UTC on 3 February (Fig. 9c), particularly in the southern sector of the TC. During this period, the dominant low-level winds shifted from southeasterly to easterly with TC propagation, with wind speeds slightly strengthening to exceed 25 m s^{-1} at 10 m altitude. Consequently, orographically induced ascent on the windward side—especially along the eastern coast—and moisture convergence on the lee side became more pronounced (moisture flux convergence ≥ 100 g m^{-3} s^{-1}; Figs. 9e–f). In contrast, in FLT_{all} (Figs. 10b–c, 10e–f), the convective regions and orographically induced wind patterns observed in CTL are absent. Instead, strengthened cyclonic winds associated with the TC's closer approach to the island are more apparent.

https://doi.org/10.5194/egusphere-2026-1893
Preprint. Discussion started: 14 April 2026

4.2 Eastern Madagascar

4.2.1 TC trajectory and intensity

An enlarged map showing the observed and simulated trajectories of TC Batsirai from CTL and sensitivity experiments around eastern Madagascar (Fig. 6b) highlights the orographically modified TC track. Similar to the behavior near Réunion Island (Fig. 6a), the simulated trajectories in FLT_{all} and FLT_{mdg} are nearly identical (green and magenta lines in Fig. 6b), whereas those in CTL and FLT_{reu} closely resemble one another (blue and orange lines) during the approach to landfall over eastern Madagascar. In both FLT_{all} and FLT_{mdg}, after passing the lee side of Réunion Island (west of ~54.5°E; see also Fig. 6a), the TC turned more directly westward until making landfall along the eastern coast of Madagascar. In contrast, a more southwestward propagation is evident in CTL and FLT_{reu}. As a result, landfall in FLT_{all} and FLT_{mdg} occurred approximately 30 km north of the location indicated by IBTrACS and simulated by CTL (black and blue solid lines).

Regarding landfall timing, in both FLT_{all} and FLT_{mdg}, TC Batsirai reached the southeastern coast (*i.e.*, near 48.5°E) at approximately 00 UTC on 5 February, about 12 hours earlier than in CTL (00 UTC *vs.* 12 UTC; green and blue lines, respectively). At landfall, nearly identical minimum MSLP value (~955 hPa) were simulated across the experiments (00 UTC on 5 February for FLT_{all} and FLT_{mdg}; 12 UTC on 5 February for CTL and FLT_{reu}; Fig. 4). The comparison between CTL and FLT_{all} suggests that the high terrain of Madagascar exerted only a minor influence on TC intensity, whereas its impact on the TC trajectory—particularly the timing and location of landfall—was more substantial. At the same time, the comparison between FLT_{mdg} and FLT_{reu} indicates that the influence of Réunion Island on the trajectory and intensity of the TC as it approached eastern Madagascar is negligible.

After landfall, the simulated trajectories of TC Batsirai in the absence of realistic Madagascar orography (*i.e.*, FLT_{all} and FLT_{mdg}) continue to propagate westward to northwestward across the island. In contrast, simulations incorporating realistic Madagascar topography (*i.e.*, CTL and FLT_{reu}, blue and orange lines in Fig. 6b) exhibit a gradual southwestward motion, consistent with the IBTrACS observation (black line).

4.2.2 Precipitation

The comparison of the five-day accumulated precipitation distributions between CTL and FLT_{all} (Figs. 7a–b) indicates that more than 1,000 mm of precipitation was concentrated at the foothills of the southeastern slope of Madagascar, of which approximately 82% (~830 mm) was induced by the high terrain. Owing to the deflected TC trajectory in the flat-terrain experiment (FLT_{all}), and additional ~220 mm of precipitation (minimum difference of –224 mm over 5 days; bluish area in Fig. 7b) was simulated along the central eastern coastal region (~20˚S). In contrast, no significant precipitation was produced over the inland region. The differences in precipitation over southeastern Madagascar between FLT_{all} and FLT_{mdg} are negligible. Likewise, the precipitation differences between CTL and FLT_{reu} are minimal, indicating that the terrain of Madagascar exerts a dominant control on the localized heavy precipitation over the southeastern slope.

Approximately 150 mm of additional precipitation is produced in FLT_{all} over the downslope of the mountainous region

https://doi.org/10.5194/egusphere-2026-1893
Preprint. Discussion started: 14 April 2026

(bluish area in Fig. 7b), resulting from the continued westward to northwestward propagation of the simulated TC across the island (Fig. 6b).

The comparison of hourly precipitation between CTL and FLT_{all} over eastern Madagascar (45.8–51.0°E, 18.2–22.8°S; see analysis domain in Fig 7) is presented in Fig. 8b. In CTL, the steep terrain produces sustained heavy precipitation (≥ 10 mm h^{-1}) for 19 consecutive hours beginning at 05 UTC on 5 February (grey-shaded period), with a peak intensity of 92.8 mm h^{-1} at 15 UTC on 5 February. In contrast, under flat-terrain conditions (FLT_{all}), heavy precipitation persists for only 4 hours and reaches a lower peak value of 44.5 mm h^{-1}. Consistent with the earlier landfall of TC Batsirai in FLT_{all}, the peak precipitation occurs earlier—at 00 UTC on 5 February, coinciding with landfall along the eastern coast—whereas in CTL the peak is observed later, at 15 UTC on 5 February. Furthermore, the precipitation differences over eastern Madagascar—particularly along the terrain foothills—between FLT_{all} and FLT_{mdg} are negligible, indicating that the terrain effect of Réunion Island has little influence on the localized precipitation over Madagascar.

4.2.3 Local dynamics

To examine the detailed orographic effects of the steep terrain of Madagascar on long-lasting localized heavy precipitation, horizontal distributions of low-level reflectivity and vertical velocity were analyzed at three selected times (01, 07, and 13 UTC on 5 February; marked by three red dots along the x-axis in Fig. 8b; see Fig. 12) and compared with simulations without realistic topography (FLT_{all}) at corresponding times when TC Batsirai is similarly situated as in CTL (16 and 22 UTC on 4 February, and 04 UTC on 5 February; Fig. 13).

At 01 UTC on 5 February, when the TC eye was located offshore of eastern Madagascar (~50.5°E, 20.5°S; Fig. 12a), it appeared relatively larger than when the storm passed near Réunion Island at 12 UTC on 3 February (Fig. 9c). An asymmetric ring of intense reflectivity (≥ 45 dBZ; Fig. 12a), accompanied by weak upward motion (≥ 0.2 m s^{-1}; yellowish region in Fig. 12d), was evident in the eyewall region over the ocean. In contrast, weakened spiral rainbands with reflectivity below 30 dBZ were observed in the southern sector of the system. Meanwhile, over the mountainous terrain (500 m topographic contour shown by the grey solid line in Fig. 12a), multiple scattered convective cells with intense reflectivity (≥ 45 dBZ) were identified. These convective regions coincided with strong low-level upward motion (≥ 1.5 m s^{-1}, reddish region in Fig. 12d). Toward this region, southeasterlies (~10 m s^{-1}) prevailed at low altitudes with Fr ~0.6, indicating that they contribute to both wind convergence and lifting along the foothills. In contrast, simulations without realistic topography (FLT_{all}) exhibit near-zero vertical velocities over eastern Madagascar (Fig. 13d) and a corresponding absence of spiral rainbands with reflectivity in the range of 20–30 dBZ in the coastal region, which are evident in CTL (delineated by the black dashed contour in Fig. 12a).

https://doi.org/10.5194/egusphere-2026-1893
Preprint. Discussion started: 14 April 2026

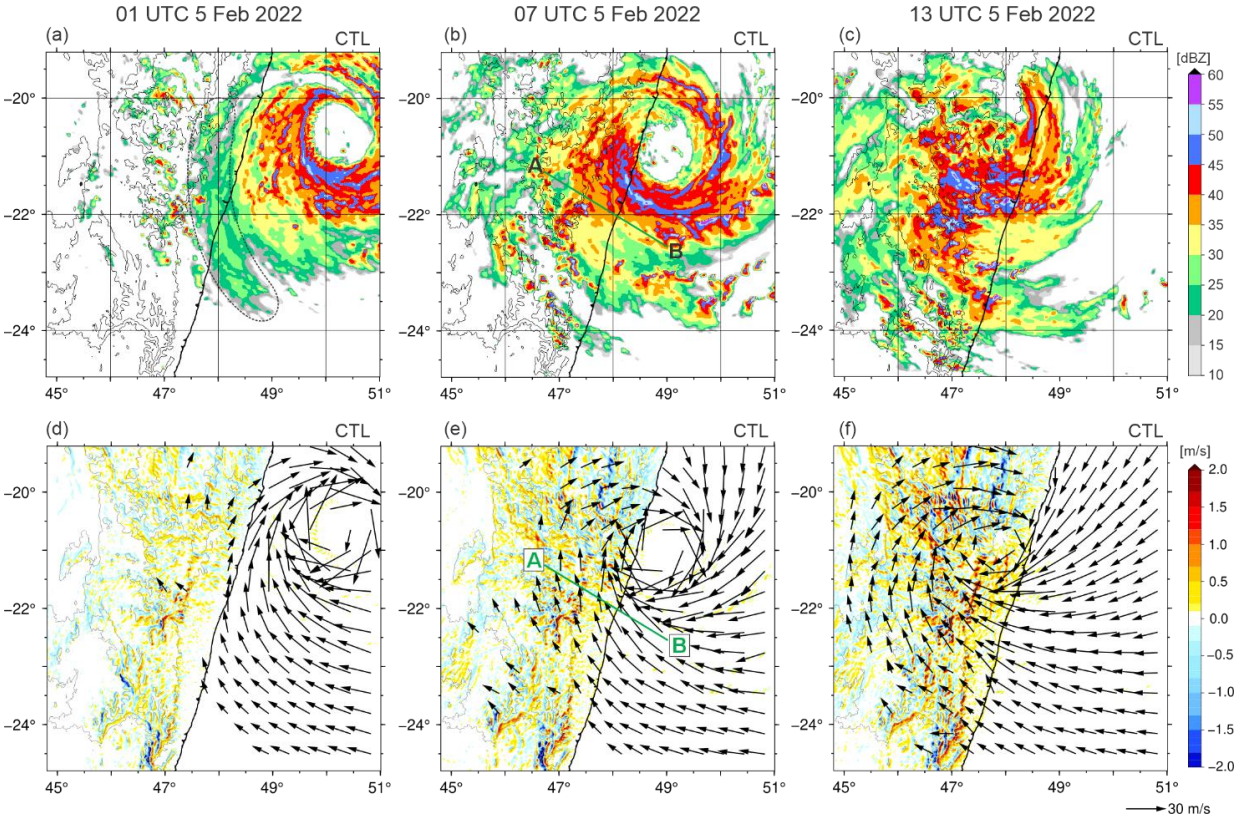

Figure 12. Horizontal distributions of CTL-simulated (a–c) reflectivity at 3 km above sea level and (d–f) vertical velocity at 20 m above sea level at 01, 07, and 13 UTC on 5 February 2022. The southeastern coastline of Madagascar is indicated by a thick solid line, and topographic contours at 500 m intervals are shown by thin solid lines in all panels. Horizontal wind vectors exceeding 10 m s^{-1} are shown. The location of the vertical cross section along A–B used in Fig. 14 is marked by a black solid line in panels (b) and (e).

https://doi.org/10.5194/egusphere-2026-1893
Preprint. Discussion started: 14 April 2026

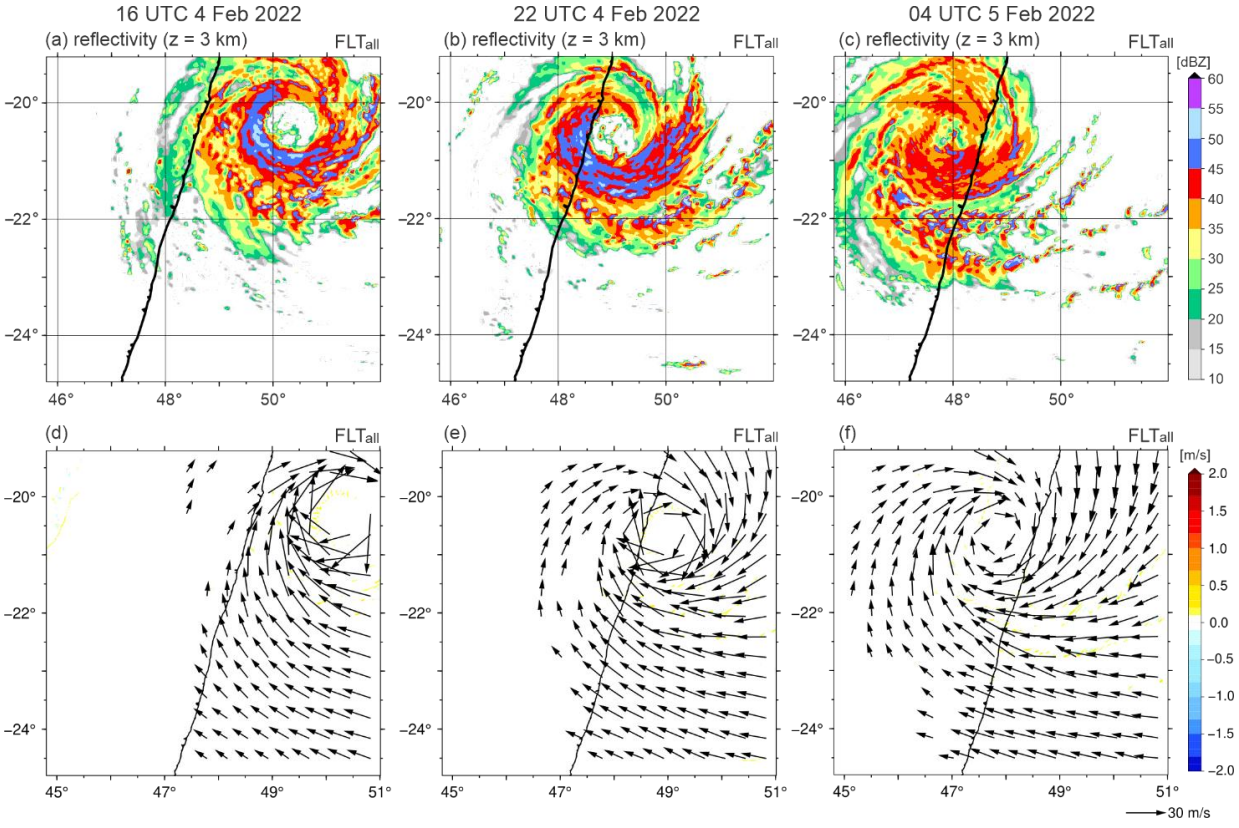

Figure 13. Same as Fig. 12, but showing results from the *FLT$_{all}$* simulation. Horizontal distributions of reflectivity at 3 km above sea level (a–c) and vertical velocity at 20 m above sea level (d–f) are shown at the corresponding times. Topographic contours, coastline, and horizontal wind vectors are displayed as in Fig. 12.

At 07 UTC on 5 February, the TC eye made landfall along the eastern coast, while an asymmetric but further thickened eyewall with intense reflectivity remained evident (Fig. 12b). In particular, in the southern half of the TC eyewall (21–22°S, 48–50°E), eyewall structures are identifiable through intense reflectivity (≥ 45 dBZ) with further strengthened upward motion (≥ 2 m s^{-1}), induced by the convergence of intensified TC-associated southeasterlies (~15 m s^{-1}) with orographically modified and weakened southerlies (~10 m s^{-1}) along the mountain foothills (Fig. 12e). Correspondingly, *Fr* increased to ~1.0. The role of terrain in generating this local wind convergence along the coastal mountainous ridge becomes more evident when compared with *FLT$_{all}$*. The simulation without realistic topography (*FLT$_{all}$*) shows homogenous strong southeasterlies (~15 m s^{-1}) associated with the TC in the eastern coastal region (Fig. 13e), and correspondingly, convective regions are absent in this region (Fig. 13b).

Horizontal and vertical cross-sections of equivalent potential temperature (θ_e) along the A-B line (marked in Fig. 12e) at 07 UTC on 5 February are shown in Fig. 14. These reveal that a large volume of warm and moist air ($\theta_e \geq 350$ K) was advected toward the southeastern coastal region by intense southeasterlies (Fig. 13a). The region of elevated θ_e extends along the coast

https://doi.org/10.5194/egusphere-2026-1893
Preprint. Discussion started: 14 April 2026

in the southern part of the TC, whereas relatively dry air ($\theta_e \leq 347$ K) is advected in the northern part. In the coastal region, three notable features are observed (Fig. 14b): (i) warm and moist air ($\theta_e \geq 350$ K) concentrated from the surface to ~1.2 km altitude, (ii) a deep warm and moist layer ($\theta_e \geq 347$ K) extending above 5 km altitude with the TC eyewall, and (iii) local wind convergence between orographically modified weaker winds and relatively stronger cyclonic easterlies below 1 km height (delineated by the grey dashed contour). Notably, at the mountain foothills, an accumulation of warm and moist air ($\theta_e \geq 350$ K) is observed from the surface up to ~2.3 km, about 1° from point A (indicated by a red arrow in Fig. 14b), whereas relatively dry air ($\theta_e \leq 347$ K, grey shading) dominates above the mountainous ridge.

The TC Batsirai made landfall along the southeastern coast around 12 UTC on 5 February, and by 13 UTC (Fig. 12c), the TC eye was no longer discernible. However, the southern portion of the cyclone (21–24°S, 46–49°E) still exhibited expanded and intensified convective regions (reflectivity ≥ 45 dBZ), particularly over mountainous terrain where strong upward motion (≥ 2 m s^{-1}) was observed, along with further strengthened horizontal winds (≥ 25 m s^{-1}; $Fr \geq 1.4$). In contrast, simulations without realistic topography (FLT_{all}) exhibit very weak upward motion (≤ 0.5 m s^{-1}) in the southern sector of the TC (yellowish area in Fig. 13f). At the same time, FLT_{all} shows (i) a reduced area with reflectivity ≥ 45 dBZ in the southern half of the cyclone, and (ii) a horizontally expanded area with reflectivity exceeding 20 dBZ (Fig. 13c). These features—including reduced convective area, expanded stratiform regions, disappearance of the eye, and asymmetric wind fields—are characteristic of the decay phase of a landfalling TC (Tuleya and Kurihara, 1978; Chan et al., 2022). Moreover, as the FLT_{all}-simulated TC propagates across Madagascar, the orographically induced scattered convective regions and intense upward motions along the mountain foothills—prominent in CTL (Figs. 12c, f)—are entirely absent in FLT_{all} (Figs. 13c, f). Similar distributions of reflectivity and vertical velocity at low altitudes are also found in FLT_{mdg}, resembling those in FLT_{all}.

https://doi.org/10.5194/egusphere-2026-1893
Preprint. Discussion started: 14 April 2026

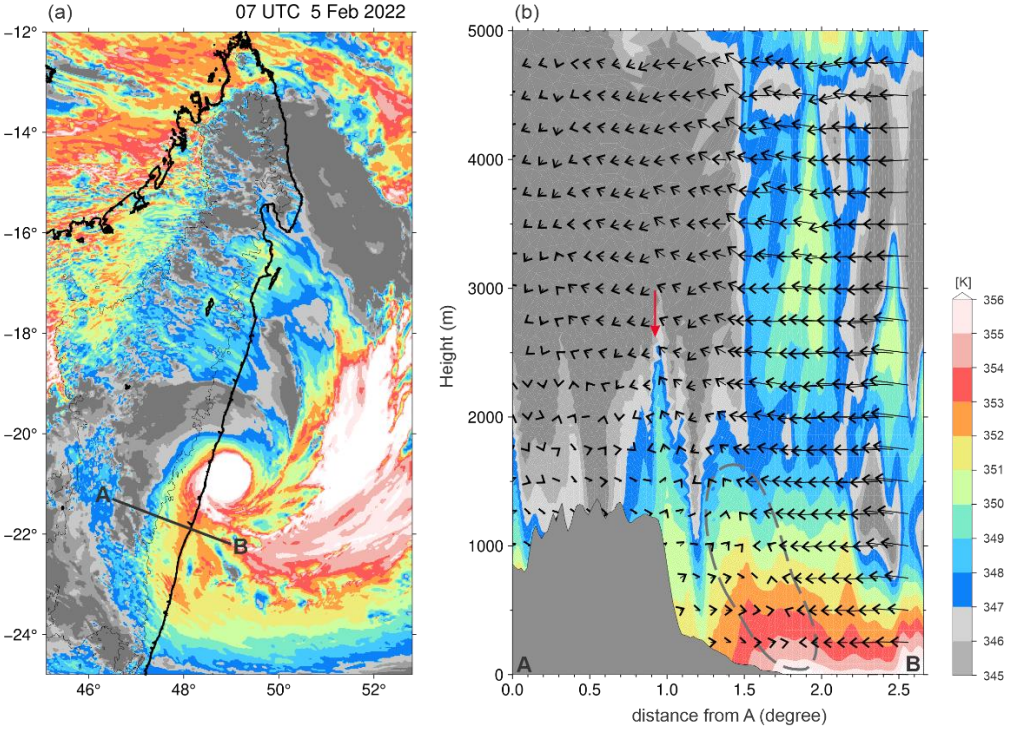

Figure 14. Horizontal and vertical distributions of CTL-simulated equivalent potential temperature (θ_e) over the Madagascar region at 07 UTC on 5 February 2022. Panel (a) shows the horizontal map with the A-B line indicating the location of the vertical cross section, which is presented in panel (b).

5 Concluding remarks

This study investigates the orographic effects of the high terrain of Réunion Island and eastern Madagascar on the lifecycle of TC Batsirai (2022) and the localized heavy precipitation that occurred during its passage. To this end, numerical simulations were performed using the Meso-NH model with a horizontal grid spacing of 2 km. To validate the simulated TC Batsirai, a combination of ground-based observations from rain gauges and dual-Doppler radars operated by Météo-France, together with spaceborne SAR data and IBTrACS best-track data, was used. Comparisons with observations demonstrate that the model successfully reproduces the lifecycle of TC Batsirai, including its trajectory and intensity evolution over the southwest Indian Ocean (SWIO), as well as the localized heavy precipitation over the mountainous regions of Réunion Island.

In addition to a control simulation (CTL), three sensitivity experiments were conducted in which the terrain was uniformly flattened over (i) the entire model domain (FLT_{all}), (ii) Madagascar only (FLT_{mdg}), and (iii) Réunion Island only (FLT_{reu}). These experiments were designed to isolate the orographic effects on heavy precipitation associated with TC Batsirai—the most intense tropical cyclone of the 2021–2022 season—during its passage near the mountainous regions of SWIO, particularly Réunion Island and eastern Madagascar. During the TC's propagation, Réunion Island was strongly affected by the passage of

https://doi.org/10.5194/egusphere-2026-1893
Preprint. Discussion started: 14 April 2026

spiral rainbands associated with the southern sector of the storm, while Batsirai eventually made landfall along the eastern coast of Madagascar.

The proportion of total precipitation induced by the steep terrain of Réunion Island (Madagascar) is estimated to be 94% (82%). Terrain-enhanced precipitation is primarily concentrated over the mountainous interior of Réunion Island and along the foothills of Madagascar. A schematic illustration (Fig. 15) depicts these intense rainfall regions using dark blue shading in both areas. In particular, intense precipitation (≥10 mm h^{-1}) persisted for 60 hours over the mountainous region of Réunion Island, of which 93%, *i.e.* 56 hours, can be attributed to the terrain effect. During this period, the peak hourly precipitation increased by 74% due to terrain effect, reaching 94 mm h^{-1} compared to 25 mm h^{-1} in the flat-terrain experiment.

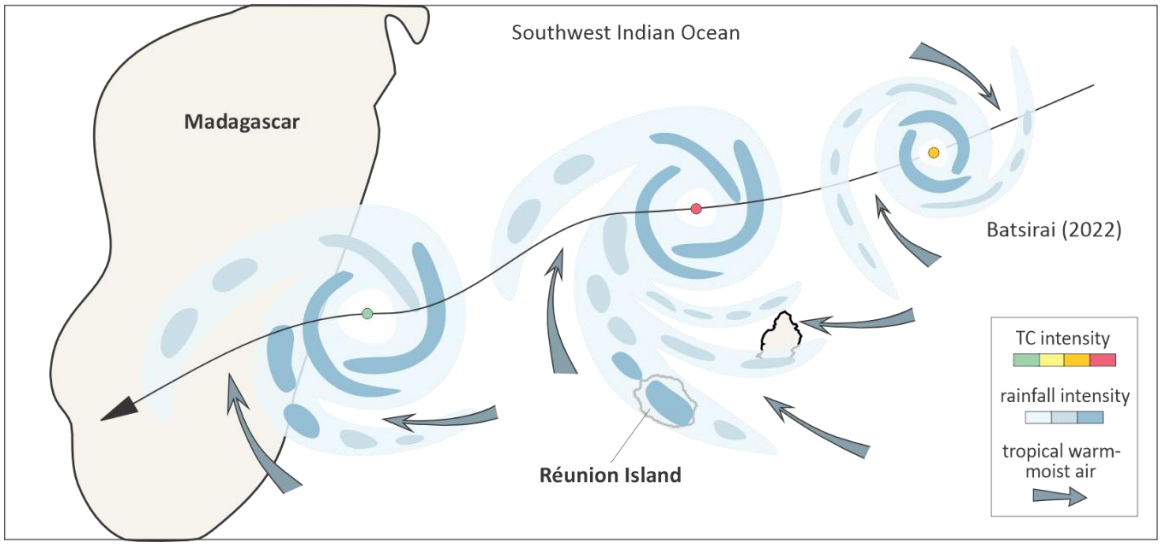

Figure 15. Schematic illustration of tropical cyclone Batsirai (2022). Rainfall intensity is indicated by a blue color scale, with darker shades representing stronger precipitation. Dark blue arrows show the warm, moist low-level flows associated with the TC, while the black arrow represents the TC trajectory.

As spiral rainbands in the southern sector of the tropical cyclone passed around Réunion Island, relatively weak low-level winds (10–12 m s^{-1}) prevailed, and the upstream *Fr* was estimated to be relatively small to moderate, ranging from 0.25 to 0.4. Under these conditions, very warm and moist air (equivalent potential temperature, $\theta_e \geq 352$ K) associated with TC Batsirai was advected toward the island by prevailing southeasterly to easterly flow at low altitudes (dark blue arrows, Fig. 15). The mountains played a key role in generating complex wind regimes, including (i) partial blocking of the flow, leading to localized wind convergence along the southeastern coast, (ii) uplift of warm and moist air to high altitudes (above 4 km) along the windward side, and (iii) convergence of warm and moist air on the lee side. Furthermore, the southwestward propagation of TC Batsirai north of Réunion Island facilitated a persistent supply of warm and moist low-level flow for more than three days, impinging on the steep slopes of the island.

https://doi.org/10.5194/egusphere-2026-1893
Preprint. Discussion started: 14 April 2026

As reported by Barbary et al. (2018), because TC Batsirai passed relatively far from the island (more than 200 km), the orographic influence of Réunion Island on modifying TC intensity and trajectory was minor. In contrast, its role in producing long-lasting localized heavy precipitation was critical. Strong low-level moisture advection toward the high terrain plays a key role in enhancing convective development within spiral rainbands. Similar mechanisms have been reported during heavy precipitation events over mountainous islands in East Asia during the monsoon season, such as the CMR of Taiwan (Jiang, 2003; Chen et al., 2004; Chien et al., 2019), Jeju Island of South Korea (Lee et al., 2014), and Yakushima Island of Japan (Kanada et al., 2000). Comparable environmental conditions favorable for convective development—such as sustained low-level moisture advection under weak-to-moderate prevailing winds and the presence of complex terrains—were also present around Réunion Island as the spiral rainbands of TC Batsirai passed nearby. Therefore, despite the noncritical proximity (*i.e.*, more than 200 km) of the TC to Réunion Island (Barbary et al., 2018), the steep terrain of this isolated island played an important role in producing rainfall intensities comparable to those in the inner eyewall region, persisting for more than three days.

The orography effect of the high terrain of Madagascar on precipitation is shown to be as critical as that observed over Réunion Island. The steep terrain of Madagascar contributes to a 78% longer duration of heavy precipitation, resulting in a total of 19 hours of intense rainfall, with a 55% increase in peak precipitation rate, reaching 93 mm h^{-1}. During this prolonged heavy-precipitation period, predominant southeasterly winds prevailed toward the mountain slopes (dark blue arrow, Fig. 15), generating strong ascending motion along the mountain foothills. Although the TC began to weaken after making landfall along the southeastern coast of Madagascar, convective activity in the southwestern sector of the storm became further enhanced, particularly near the mountain foothills (dark blue shading, Fig. 15). As TC Batsirai approached eastern Madagascar, low-level easterlies strengthened, exceeding of 20 m s^{-1}, and the upstream *Fr* was correspondingly estimated to be relatively high, ranging from 0.6 to 1.4. Under these conditions of relatively strong low-level prevailing winds, pronounced orographically induced low-level ascent occurred along the eastern foothills of Madagascar, resulting in the uplift of warm and moist air ($\theta_e \geq 352$ K) to higher altitudes.

Unlike the case of Réunion Island, the orographic influence of Madagascar was critical not only for localized heavy precipitation but also for the trajectory of TC Batsirai, particularly with respect to the timing and location of landfall. In terms of timing, the presence of the large-scale mountainous terrain of Madagascar (about 1,600 km long; 600 km wide, and 2,800 m high) plays a key role in blocking the environmental southeasterly flow, particularly in the southern sector of the storm, thereby decelerating the low-level southeasterlies over the southern part of the island. This interaction between the large-scale terrain and the environmental flow contributes to delaying TC landfall. Moreover, the deceleration of the environmental southeasterly flow appears to contribute to a southward shift in the TC landfall location by approximately 30 km.

In this study, we thoroughly examined the roles of Réunion Island and Madagascar in generating localized heavy precipitation during the passage of an intense TC using both observations and a high-resolution numerical model. Based on the present results, further investigations of terrain effects associated with intense TCs approaching Réunion Island and Madagascar from different directions (*e.g.*, southward and southeastward tracks) and at varying proximities would help

https://doi.org/10.5194/egusphere-2026-1893
Preprint. Discussion started: 14 April 2026

advance our understanding of TC–orography interactions in the region. In addition, the influence of the complex orography of Réunion Island—including steep topography, valleys, and surrounding bathymetry—on the mechanisms enhancing localized intense precipitation over the southern part of the island warrants further investigation. Furthermore, with regard to the genesis of TC Batsirai, the equatorial Rossby wave appears to have played a dominant role among the sub-seasonal drivers, compared with other modes such as Madden-Julien Oscillation and Kelvin waves (data not shown). The influence of equatorial Rossby waves on modulating TC genesis and trajectory in the SWIO would therefore be an interesting topic for future research.

On the other hand, studies on intense TCs and their long-term evolution in the SWIO basin remain relatively limited compared with those conducted in other TC-active basins, such as the northwestern Pacific Ocean and the North Atlantic, mainly due to the limited availability of observations and research resources. As in other TC-active basins, TC activity in the SWIO is expected to evolve throughout the century in response to climate change and increasing greenhouse gas concentrations (Emanuel 2005; Knutson et al., 2013; Cattiaux et al., 2020). Using state-of-the-art climate models with horizontal resolution typically finer than 50 km, Cattiaux et al. (2020) reported that in a 2 K warmer climate, the frequency of TCs may decrease by approximately 20%, while their maximum lifetime intensity is projected to increase, accompanied by a slight poleward shift in TC tracks and a substantial delay (about one month) in the onset of the cyclone season. Specifically for the SWIO basin, Cattiaux et al. (2020) indicated that the time-averaged sea surface temperature (SST) in the future period (2051–94) is projected to warm by approximately 1.6–2 K relative to the present climate (1971–2014), with a basin-wide mean warming of about 1.8 K. In this context, future studies should examine in greater detail how the increased thermodynamic energy released from warmer SST—particularly from the upper ocean layer—may influence the TC lifecycle. Such changes could, in turn, modify the spatial distribution, duration, and intensity of heavy precipitation over mountainous regions such as Réunion Islands and Madagascar.

Code and data availability

Meso-NH output data are available from Lee, K.-O. upon request.

Author contributions

This work was carried out through a collaborative effort. KOL designed and performed the numerical simulations. SB provided guidance on model compilation and the preparation of the numerical experiments. KH developed the Python scripts for data

https://doi.org/10.5194/egusphere-2026-1893
Preprint. Discussion started: 14 April 2026

analysis, and CS analyzed the SAR wind comparisons with the model. RL reviewed the manuscript, while KOL prepared the manuscript with contributions from all co-authors.

Competing interests

The authors declare that they have no conflict of interest.

Acknowledgements

The authors express our gratitude to Dr. S. Shimizu, Dr. T. Maesaka, and colleagues at the National Research Institute for Earth Science and Disaster Resilience (NIED), Tsukuba, Japan, for their valuable suggestions. We also thank T. Kriat and S. Langlade of Météo-France for their insightful discussions. Numerical simulations were performed using the Météo-France supercomputing system, Belenos. Meteorological analysis data were provided by the European Centre for Medium-Range Weather Forecasts, and the hurricane track data were obtained from the IBTrACS archive (ncdc.noaa.gov/ibtracs/).

Financial support

Support funds and grant agreement numbers are listed as specified upon manuscript registration and reported to FundRef upon publication.

References

Arivelo, T. and Lin, Y.-L.: Climatology of heavy orographic rainfall induced by tropical cyclones over Madagascar: From synoptic to mesoscale perspectives, Earth Science Research, 5 (2), doi:10.5539/esr.v5n2p132, 2016.

Barbary, D., Leroux, M.-D., and Bousquet, O.: The orographic effect of Réunion Island on tropical cyclone track and intensity, Atmos. Sci. Lett., 20:e882, doi:10.1002/asl.882., 2018.

Bender, M. A., Tuleya R. E., Kurihara, Y.: A numerical study of the effect of a mountain-range on a landfalling tropical cyclone. Mon. Wea. Rev., 113: 567−582, 1985.

Bender, M. A., Tuleya R. E., Kurihara, Y.: A numerical study of the effect of island terrain on tropical cyclones. Mon. Wea. Rev., 115: 130−155, 1987.

Cattiaux, J., Chauvin, F., Bousquet, O., Malardel, S., Tsai, C. L. : Projected changes in the southern Indian ocean cyclone activity assessed from high-resolution experiments and CMIPS models. J. Climate, 33, 4975–4991, 2020.

Chan, K. T. F., Zhang, K., Wu, Y., and Chan, J. C. L: Landfalling hurricane track modes and decay. Nature, 606, E7−E11, https://doi.org/10.1038/s41586-020-2867-7, 2022.

https://doi.org/10.5194/egusphere-2026-1893
Preprint. Discussion started: 14 April 2026

Chang, C. P., Yeh, T. C., Chen, J. M.: Effects of terrain on the surface-structure of typhoons over Taiwan. Mon. Wea. Rev. 121, 734−752, 1993.

Chen, T.C., Wang, S.Y., Huang, W.R., and Yen, M.C.: Variation of the East Asian Summer Monsoon rainfall, J. Climate, 17 (4), 744–762, doi:10.1175/1520-0442(2004)017<0744:VOTEAS>2.0.CO;2, 2004.

Cheng, L.-W., Yu, C.-K., and Chen, S.-P.: Identifying mechanisms of tropical cyclone generated orographic precipitation with Doppler radar and rain gauge observations. Climate and Atmospheric Science, 8:35, doi:10.1038/s41612-025-00921-4. 2025.

Chien, F.C., and Chiu, Y.C.: A composite study of southwesterly flows and rainfall in Taiwan, J. Meteorol. Soc. Jpn, 97, 1023−1040, doi:10.2151/jmsj.2019-057, 2019.

Colella, P. and Woodward, P.R: The piecewise parabolic method (PPM) for gas dynamical simulations, J. comput. Physc., 54, 174−201, doi:10.1016/0021-9992(84)90143-8, 1984.

Combot, C., Mouche, A., Knaff, J., Zhao, Y., Zhao, Y., Vinour, L., Quilfen, Y., and Chapron, B.: Extensive high-resolution Synthetic Aperture Radar (SAR) data analysis of Tropical Cyclones: comparisons with SFMR flights and Best-Track. Mon. Wea. Rev., 148(11), 4545-4563, doi:10.1175/MWR-D-20-0005.1, 2020.

Cuxart, J., Bougeault, P., and Redelsperger, J. L.: A turbulence scheme allowing for mesoscale and large-eddy simulations. Q. J. R. Meteorol. Soc., 126(562): 1−30, doi:10.1002/qj.49712656202, 2000.

Davies, H: A lateral boundary formulation for multi-level prediction models, Q. J. Roy. Meteor. Soc., 102, 405−418, 1976.

Duchiron, B.: Variabilité interannuelle de la pluviométrie dans l'espace riverain de l'Océan Indien. Thèse de doctorat de l'université de Paris 7, 272p., 2002.

Duffourg, F., Lee, K.-O., Ducrocq, V., Flamant, C., Chazette, P., and Girolamo, P.: Role of moisture patterns in the backbuilding formation of HyMeX IOP13 Heavy precipitation systems., Q. J. R., Meteorol. Soc., 144, 291−303, doi:10.1002/qj.3201, 2018.

Dyson, L: Heavy daily-rainfall characteristics over the Gauteng Province, Water SA, 35(5), doi:10.4314/wsa.v35i5.49188, 2009.

Emanuel, K. A.: Increasing destructiveness of tropical cyclones over the past 30 years. Nature, 436, 686−688, doi:10.1038/nature03906., 2005.

Fitchett, J.M, and Grab, S.W: A 66-year tropical cyclone record for South-East Africa: temporal trends in a global context. Int J. Climatol, 34:3604−3615, doi:10.1002/joc.3932, 2014.

Gahtan, J., Knapp, K. R., Schreck, C. J., Diamond, H. J., Kossin, J. P., and Kruk, M. C.: International best track archive for climate stewardship (IBTrACS) project, Version 4r01. NOAA national centers for environmental information, doi:10.25921/82ty-9e16, 2024.

Gal-Chen, T. and Somerville, R. C. J.: On the use of a coordinate transformation for the solution of the Navier-Stokes equations. J. Comput. Phys. 17: 209−228, doi:10.1016/0021-9991(75)90037-6, 1975.

Grodsky, S. A. and Carton, J. A.: The intertropical convergence zone in the south Atlantic and the Equatorial cold tongue, Journal of Climate, 16, 723−733, doi:10.1175/1520-0442(2003)016<0723:TICZIT>2.0.CO;2, 2003.

https://doi.org/10.5194/egusphere-2026-1893
Preprint. Discussion started: 14 April 2026

Hamuro, M. et al. Precipitation bands of Typhoon Vera in 1959 (Part 1). J. Meteor. Soc. Japan. **47**, 298–308, 1969.

Hastenrath, S. and Lamb, P.: On the dynamics and climatology of surface flow over the Equatorial ocean. Tellus, 30 (5) 436–448, doi:10.1111/j.2153-3490.1978.tb00859.x, 1978.

Huang, C.-Y., Chou, C.-W., Chen, S.-H., and Xie, J.-H., Topographic rainfall of tropical cyclones past a mountain range as categorized by idealized simulations, Weather and Forecasting, 35(1), 25–47, doi:10.1175/WAF-D-19-0120.1, 2020.

Jiang, Q.: Moist dynamics and orographic precipitation, Tellus, 55A, 301−316, 2003.

Jolivet, S., Chan-Ming, F., Barbary, D., and Roux, F.: A numerical study of orographic forcing on TC Dina (2002) in South West Indian Ocean, Ann, Geophys., 31, 107–125, doi:10.5194/angeo-31-107-2013, 2013.

Kanada, S., Minda, H., Geng, B., Takeda, T.: Rainfall enhancement of band-shaped convective cloud system in the downwind side of an isolated island. J. Meteor. Soc. Japan, 78, 47−67, 2000.

Kantha, L.: Time to replace the Saffir-Simpson hurricane scale? Eos, 87, 3−6, doi:10.1029/2006EO010003, 2006.

Khan, M.J.U., Durand, F., Afroosa, M., Coulet, P., Bertin, X., Mueller, V., Krien, Y., and Wainwright, C.: Tropical cyclone induced compound flooding in Madagascar: a coupled modeling approach., Nat Hazards, 121:11013−11050, doi:10.1007/s11069-025-07209-z, 2025.

Knapp, K. R., Kruk, M. C., Levinson, D. H., Diamond, H. J., Neumann, C. J.: The international best track archive for climate stewardship (IBTrACS): Unifying tropical cyclone best track data. Bull. Amer. Meteor. Soc., 91, 363−376. Doi:10.1175/2009BAMS2755.1, 2010.

Knutson, T. R., and coauthors: Dynamical downscaling projections of twenty-first-century Atlantic hurricane activity: CMIP3 and CMIP5 model-based scenarios. J. Climate, 26, 6591–6617, doi:10.1175/JCLI-D-12-00539.1., 2013.

Kruk, M. C., Knapp, K. R., and Levinson, D. H.: A technique for merging global tropical cyclone best track data. J. Atmos. Oceanic Technol., 27, 680−692, doi:10.1175/2009JTECHA1267.1, 2010.

Lac, C., Chaboureau, J. P., Masson, V., Pinty, J. P., Tulet, P., Escobar, J., Leriche, M., Barthe, C., Aouizerats, B., Augros, C., Aumond, P., Auguste, F., Bechtold, P., Berthet, S., Bieilli, S., Bosseur, F., Caumont, O., Cohard, J. M., Colin, J., Couvreux, F., Cuxart, J., Delautier, J., Dauhut, T., Ducrocq, V., Filippi, J.B., Gazen, D., Geoffroy, O., Gheusi, F., Honnert, R., Lafore, J. P., Lebeaupin, Brossier C., Libois, Q., Lunet, T., Mari, C., Maric, T., Mascart, P., Mogé, M., Molinié, G., Nuissier, O., Pantillon, F., Peyrillé, P., Pergaud, J., Perraud, E., Pianezze, J., Redelsperger, J. L., Ricard, D., Richard, E., Riette, S., Rodier, Q., Schoetter, R., Seyfried, L., Stein, J., Suhre, K., Taufour, M., Thouron, O., Turner, S., Verrelle, S., Vié, B., Visentin, F., Vionnet, V., and Wautelet, P.: Overview of the Meso-NH model version 5.4 and its applications. Geosci. Model Dev., 11, 1929-1969, 2018.

Le Quotidien: Batsirai, 47 millions de pertes agricoles. https://www.lequotidien.re/article/actualites/2022/02/11/batsirai-47-millions-de-pertes-agricoles. Accessed 31 March 2026, 2022.

Lee, K. O., Uyeda, H., Shingo, S., Lee, D. I.: Dual-Doppler radar analysis of the enhancement of a precipitation system on the northern side of Mt. Halla, Jeju Island, Korea on 6 July 2007. Atmos. Res., 118 (2012), 133–152, doi:10.1016/j.atmosres.2010.06.017., 2012.

https://doi.org/10.5194/egusphere-2026-1893
Preprint. Discussion started: 14 April 2026

Lee, K. O., Uyeda, H., and Lee, D. I.: Effect of an isolated elliptical terrain (Jeju Island) on rainfall enhancement in a moist environment, Tellus A, 66, 20484, doi:10.3402/tellusa.v66.20484, 2014.

Lee, K. O., Flamant, C., Ducrocq, V., Duffourg, F., Fourrié, N, Delanoë, J., Bech, J.: Initiation and development of a mesoscale convective system in the Ebro River Balley and related heavy precipitation over northeastern Spain during HyMeX IOP15a, Q. J. R. Meteorol. Soc., doi:10.1002/qj.2978, 2017.

Lee, K. O., Flamant, C., Duffourg, F., Ducrocq, V., Chaboureau, J.P. : Impact of upstream moisture structure on a back-building convective precipitation system in south-eastern France during HyMeX IOP13, Atmos. Chem. Phy., 18, 16845−16862, doi:10.5194/acp-18-16845-2018, 2018.

Lin, Y.-L, and Crosby Savage III, L: Effects of landfall location and the approach angle of a cyclone vortex encountering a mesoscale mountain range. J. Atmos. Sci., 68, 2095–2106, doi:10.1175/2011JAS3720.1. 2011.

Lin, Y. L., Ensley, D. B., Chiao, S. and co-authors: Orographic influences on rainfall and track deflection associated with the passage of a tropical cyclone. Mon. Wea. Rev., 130: 2929−2950, 2002.

Lin, Y. L., Chen, S. Y., Hill, C. M, and co-authors: Control parameters for the influence of a mesoscale mountain range on cyclone track continuity and deflection. J. Atmos. Sci., 62: 1849−1866, 2005.

Lin, Y.-F., Wu, C.-C., Yen, T.-H., Huang, Y.-H., and Lien, G.-Y., Typhoon Fanapi (2010) and its interaction with Taiwan terrain – Evolution of the uncertainty in track, intensity and rainfall simulations, doi:10.2151/jmsj.2020-006, 2020.

Masson, V., Le Moigne, P., Martin, E., Faroux, S., Alias, A., Alkama, R., Belamari, S., Bardu, A., Boone, A., Bouyssel, F., Brousseau, P., Brun, E., Calvet, J.C., Carrer, D., Decharme, B., Delire, C., Donier, S., Essaouini, K., Gibelin, A. L., Gior dani, H., Habets, F., Jidane, M., Kerdraon, G., Kourzeneva, E., Lafaysse, M., Lafont, S., Lebeaupin, BC., Lemonsu, A., Mah fouf, J.F., Marguinaud, P., Mokhtari, M., Morin, S., Pigeon, G., Salgado, R., Seity, Y., Taillefer, F., Tanguy, G., Tulet, P., Vincen don, B., Vionnet, V., and Voldoire, A.: The surfex v7.2 land and ocean surface platform for coupled or offline simulation of earth surface variables and fluxes, Geosci. Model Dev., 6, 929–960, doi:/10.5194/gmd-6-929-2013, 2013.

Mlawer, E. J., Taubman, S. J., Brown, P. D., Iacono, M. J., and Clough, S. A.: Radiative transfer for inhomogeneous atmospheres: RRTM, a validated correlated-k model for the longwave, J. Geophys. Res., 102, 16663−16682, 1997.

Mouche A., Chapron, B., Knaff, J., Zhao, Y., Zhang, B., and Combot, C.: Copolarized and Cross-Polarized SAR Measurements for High-Resolution Description of Major Hurricane Wind Structures: Application to Irma Category 5 Hurricane. Journal Of Geophysical Research-oceans, 124(6), 3905−3922. doi:10.1029/2019JC015056, 2019.

Neeham, H. F., Keim B. D., and Sathiaraj, D.: A review of tropical cyclone-generated storm surges: global data sources, observations, and impacts. Rev. Geophys, 53: 545−591, doi:10.1002/2014rg000477, 2015.

Masson, V., Le Moigne, P., Martin, E., Faroux, S., Alias, A., Alkama, R., Belamari, S., Bardu, A., Boone, A., Bouyssel, F., Brousseau, P., Brun, E., Calvet, J.C., Carrer, D., Decharme, B., Delire, C., Donier, S., Essaouini, K., Gibelin, A. L., Giordani, H., Habets, F., Jidane, M., Kerdraon, G., Kourzeneva, E., Lafaysse, M., Lafont, S., Lebeaupin, BC., Lemonsu, A., Mahfouf, J.F., Marguinaud, P., Mokhtari, M., Morin, S., Pigeon, G., Salgado, R., Seity, Y., Taillefer, F., Tanguy, G., Tulet, P.,

https://doi.org/10.5194/egusphere-2026-1893
Preprint. Discussion started: 14 April 2026

Vincendon, B., Vionnet, V., and Voldoire, A.: The surfex v7.2 land and ocean surface platform for coupled or offline simulation of earth surface variables and fluxes. Geosci. Model Dev. 6(4): 929−960, doi:10.5194/gmd-6-929-2013, 2013.

OCHA: Southern Africa: cyclone season flash update no. 6 (Tropical Cyclone Batsirai) (7 February 2022). https://web.archive.org/web/20220214103935/https://floodlist.com/africa/madagascar-death-cyclone-batsirai-update-february-2022, accessed 31 March 2026, 2022.

Parrish, J. R., Burpee, R. W., and Marks, F. D. Jr.: Rainfall patterns observed by digitized radar during the landfall of Hurricane Frederic (1979). Mon. Wea. Rev. 1933–1944, 1982.

Pinty, J. P. and Jabouille, P.: A mixed-phased cloud parametrization for use in a mesoscale non-hydrostatic model: Simulations of a squall line and of orographic precipitation. In: Proc. Of the Conference on Cloud Physics. Amer. Meteorol. Soc, Boston: Everett, WA, USA, 17−21 Aug. 1998. Pp. 217−220, 1998.

Rakotoarimanana, Z. M. H., Rakotoarimanana, Z. H., Pandin, M. G. R., and Waloejo, C. S.: Analysis of tropical cyclones 2000−2020 in Madagascar, Disaster Advances, 15 (3), 2022.

Romatschke, U., Medina, S., and Houze, R.A.: Regional, seasonal, and diurnal variations of extreme convection in the south Asian region, J. Climate, 23 (2), 419−439, doi:10.1175/2009JCLI3140.1, 2010.

Roux, F., Chang-Min, F., Lasserre-Bigorry, A., and Nuissier, O.: Structure and evolution of intense tropical cyclone Dina near La Réunion on 22 January 2022: GB-EVTD analysis of single Doppler radar observations. J. of Atmospheric and oceanic Technology, 21, 1501−1518, doi:10.1175/1520-0426(2004)021<1501:SAEOIT>2.0.CO;2, 2004.

Tuleya, R. E. and Kurihara, Y.: A numerical simulation of the landfall of tropical cyclones. J. Atmos. Sci., 35, 242–257, 1978.

Wu, C.-C.: Numerical simulation of Typhoon Gladys (1994) and its interaction with Taiwan terrain using the GFDL hurricane model. Mon. Wea. Rev., 129, 1533–1549, 2001.

Wu, C. C., and Kuo Y. H.: Typhoons affecting Taiwan: Current understanding and future challenges. Bull. Amer. Meteor. Soc., 80: 67−80, 1999.

Wu, C.-C., Yen, T.-H., Huang, Y.-H., Yu, C.-K., and Chen, S.-G. Statistical characteristic of heavy rainfall associated with typhoons near Taiwan based on high-density automatic rain gauge data. Bull. Amer. Meteor. Soc. 97, 1363–1375, 2016.

Wu, Y.-C., Yang, M.-J., and Rogers, R. F.: Examining terrain effects on the evolution of precipitation and vorticity of typhoon Fanapi (2010) after departing the central mountain range of Taiwan, Mon. Wea. Rev., doi:10.1175/MWR-D-21-0205.1, 2022.

Yeh, T. C. and Elsberry, R. L.: Interaction of typhoons with the Taiwan orography. Part I: Upstream track deflections. Mon. Wea. Rev., 121: 3193−3212, 1993a.

Yeh, T. C., and Elsberry, R. L.: Interaction of typhoons with the Taiwan orography. Part II: Continuous and discontinuous tracks across the island. Mon. Wea. Rev., 121:3213−3233, 1993b.

Yu, C.-K., and Cheng, L.-W.: Distribution and mechanism of orographic precipitation associated with typhoon Morakot (2009). J. Atmos. Sci., 70, 2894−2915, 2014.